scientific reports



OPEN

Deciphering the collisional dynamics of the Bangong-Nujiang Tethyan Ocean: multiregional anisotropy of magnetic susceptibility (AMS) constraints from the Central Tibetan Plateau

Qinglong Chen^{1,2 \boxtimes}, Xin Cheng², Nan Jiang³, Bitian Wei², Longyun Xing², Dongmeng Zhang², Ruiyang Chai² & Hanning Wu^{2 \boxtimes}

The Middle Jurassic to Late Cretaceous interval marks a pivotal geological timeframe, encompassing both the progressive amalgamation of the Lhasa and Qiangtang Blocks and the terminal closure of the Bangong-Nujiang Tethyan Ocean. Investigating the closure evolution of the Bangong-Nujiang Tethyan Ocean during the Middle Jurassic to Late Cretaceous period will significantly enhance our understanding of the broader tectonic dynamics within the Global Tethys Domain. To elucidate the subduction polarity and timing of the closure of the Bangong-Nujiang Tethyan Ocean during this critical period, this study builds upon previous investigations of magmatic activity, stratigraphic sedimentary features, and paleomagnetic data. By conducting zircon U-Pb geochronology and systematic anisotropy of magnetic susceptibility (AMS) analyses across the Lhasa Block, Qiangtang Block, and Bangong-Nujiang suture zone, the following insights were obtained: (1) The northward compressional movement of the Southern Qiangtang Block during the Middle-Late Jurassic is attributed to the northward subduction of the Bangong-Nujiang Tethyan Ocean. While the southward compressional movement of the Southern Lhasa Block during the Cretaceous is associated to the southward subduction of the same oceanic domain. (2) The volcanic breccia and detrital sandstone examined in this study are hosted within the lower part of the Shamuluo Fm., yielding a depositional age of 112-95 Ma. This temporal window corresponds to a critical transition period during which the Bangong-Nujiang Tethyan Ocean underwent a fundamental shift in subduction polarity from northward to southward. (3) The Bangong-Nujiang Tethyan Ocean initially underwent northward subduction during the Mid-Late Jurassic, followed by a tectonic polarity reversal (~112-102.9 Ma) spanning the Late Jurassic to Early Cretaceous transition, ultimately establishing southward subduction patterns by the Early Cretaceous. The southward subduction persisted until the Early Shexing Fm. (~103.8-92 Ma), with its cessation marking the complete tectonic amalgamation between the Lhasa and Qiangtang Blocks.

Keywords Bangong-Nujiang Tethyan ocean, Closure evolution, Anisotropy of magnetic susceptibility (AMS), Zircon U-Pb geochronology

The formation and evolution of the Tibetan Plateau initiated with the breakup of the Gondwana Continent, which was accompanied by the gradual northward drift of the landmasses and the collision with the Eurasia, as well as the closure of the Paleo and Neo-Tethys Oceans. The Tibetan Plateau preserves a comprehensive record of major geological events throughout its history of crustal thickening and compressional uplift, with two particularly significant tectonic events standing out in its evolutionary history. The first is the continent-continent collision

¹College of Materials Science and Engineering, Xi'an Shiyou University, Xi'an 710065, China. ²Department of Geology, Northwest University, Xi'an 710069, China. ³School of Petroleum Engineering and Environmental Engineering, Yan' an University, Yan' 716000, China. [⊠]email: chenqinglong@stumail.nwu.edu.cn; wuhn2506@nwu.edu.cn

between the Indian Plate and Eurasia, which generated extensive magmatic rock exposures along the southern margin of the Gangdise Belt. The second, occurring earlier at 110-100 Ma, involved the collision of the Lhasa and Qiangtang Blocks accompanied by the closure of the Bangong-Nujiang Tethyan Ocean. This event triggered widespread magmatic activity, evidenced by substantial outcrops along the northern and central margins of the Lhasa Block and within the Qiangtang Block. The collision of the Indian plate with Eurasia is related to the closure of the Yarlung-Zangbo Neo-Tethys Ocean, and studies have shown that the Yarlung-Zangbo Neo-Tethys Ocean has always been subducted in the north direction, and that the subduction polarity has never changed. Research on magma geochemistry indicates that magmatism in the southern and central parts of the Lhasa Block during the Early-Middle Jurassic, as well as the Lhasa Block in the Cretaceous, is related to northward subduction of the Neo-Tethys Ocean^{2,3}. However, the subduction process of the Bangong-Nujiang Tethyan Ocean still remains controversial. Accompanied by numerous studies, it is now mainly believed that bidirectional subduction exists in the Bangong-Nujiang Tethyan Ocean (Fig. 1a). Magmatism in the northern and central Lhasa Block from the Middle Jurassic to the Cretaceous is related to southward subduction of the Bangong-Nujiang Tethyan Ocean⁴. In addition, based on the study of the less exposed Mesozoic magmatism in the South Qiangtang Block, it is suggested that the magmatism from the Late Jurassic to the Early Late Cretaceous was related to the northward subduction of the Bangong-Nujiang Tethyan Ocean⁵. However, exactly how and when the Bangong-Nujiang Tethyan Ocean changes its subduction polarity is still not completely resolved (Fig. 1b).

Consequently, this region has been extensively investigated through multiple geological approaches, including tectonic paleomagnetism, ophiolite studies, and sedimentary analyses. Paleomagnetic investigations, in particular, provide crucial constraints on plate positions through the calculation of paleolatitudes from remnant magnetization. According to the types of ophiolites (SSZ, MORB, etc.), the time of oceanic expansion and closure can be inferred (Fig. 1c). The ocean-land transition is limited by the contact relationships between strata and the depositional environments in which the strata are developed. The tectonic evolution of the Bangong-Nujiang Tethyan Ocean consists of three processes: expansion, subduction and closure. And the specific scientific issues include the time of its expansion and closure, as well as the process of oceanic subduction. Researches on time of ocean opening, based on ophiolite studies⁶, it suggests that the Bangong-Nujiang Ocean was already expanding in the Late Permian⁵. Combined with the intrusive basaltic complexes of the South Qiangtang Block (279-258Ma)⁷ and the one in the North Lhasa Block (278Ma)⁸, as well as the paleontological evidence on both sides of the Bangong-Nujiang suture zone, it is suggested that the Bangong-Nujiang Ocean was already expanding before 260 Ma. The discussion on the closure time of oceanic basin, based on studies of paleomagnetism, it suggested that closure of the Bangong-Nujiang Ocean occurred before the Early Cretaceous^{9–14}. The unconformity contact developed on the pre-arc basin of the South Qiangtang Block (-166Ma)¹⁵ and the non-marine stratigraphic transition in the Nyima area (125-118Ma)¹⁶suggest that the Lhasa Block and the Qiangtang Block collided at 150-140 Ma.

The tectonic evolution of the Bangong-Nujiang Tethyan Ocean has been constrained through anisotropy of magnetic susceptibility (AMS) studies, which provide critical insights into regional tectonic deformation patterns. The essence of magnetic fabric is the study of tectonic stress or flow by the preferred orientation of magnetic minerals, particles or lattices in rocks¹⁷. This method has a widespread application in the field of tectonic geology and also in the study of tectonic environments. In AMS research, the maximum axis (Kmax) is perpendicular to the bedding plane, and the direction of magnetic lineation is parallel to the direction of minor principal stress, indicating that it was formed in an extensional environment 18,19. The distribution of (Kmax) is concentrated and extends along the strata, indicating that it was formed in a compressional environment^{19,20}. And due to the good correspondence between the strain ellipsoid and the magnetization ellipsoid, the magnetic lineation corresponds to the direction of palaeostress after rotation²¹, and the Kmin represents the direction of maximum compressive stress²². Moreover, there are six types of magnetic fabric in the evolution process of AMS²³, including sedimentary fabric, initial deformation fabric, pencil-shaped fabric, weak cleavage fabric, strong cleavage fabric, and stretching lineation fabric. The application of AMS in the Tibetan Plateau is also gradually advancing. Existing studies have investigated key tectonic features, including the Gonjo Basin for dating Tibetan Shortening²⁴, the Zaduo limestone for oroclinal bending constraints²⁵, the Longmen Mountain area²⁶ and the Zedang thrust fault system for tectonic deformation analysis²⁷. The above research has obtained results in regional deformation patterns, direction transition of stress field, as well as collision and uplift of the Himalayas. However, the method of AMS to study the Central Tibetan Plateau is still blank. Therefore, conducting detailed AMS research on the Lhasa Block and Qiangtang Block is of great significance for further studying the tectonic deformation and uplift evolution of the Tibetan Plateau.

By integrating AMS analysis with zircon U-Pb geochronology, this study conducts a comprehensive stress field investigation on the continuous Middle Jurassic to Late Cretaceous sedimentary sequences in the Central Tibetan Plateau. The systematic analysis of stratigraphic chronology and comparative study of contemporaneous stress orientations enable the reconstruction of stress regimes and kinematic mechanisms governing the Lhasa and Qiangtang Blocks during the Middle Jurassic-Late Cretaceous interval. Furthermore, based on precise geochronological data from the Shamulo Fm. within the Bangong-Nujiang suture zone, this research provides critical constraints on the evolutionary history and closure processes of the Bangong-Nujiang Tethyan Ocean.

Geological backgroud

The formation and evolution process of the Qinghai-Tibet Plateau includes processes such as continental breakup, oceanic expansion, oceanic subduction and continental collision, etc²⁸. The rapid breakup of the Cimmerian Continent from the Gondwanaland resulted in its collision with Eurasia in the Late Triassic, leading to the closure of the Paleo-Tethys Ocean. The Lhasa Block drifted northward during the Triassic and collided with the Qiangtang Block during the Early Cretaceous, resulting in the closure of the Bangong-Nujiang Tethyan Ocean²⁹. Subsequently, the Indian Continent drifted northward, and the Himalayan Terrane collided with the Lhasa

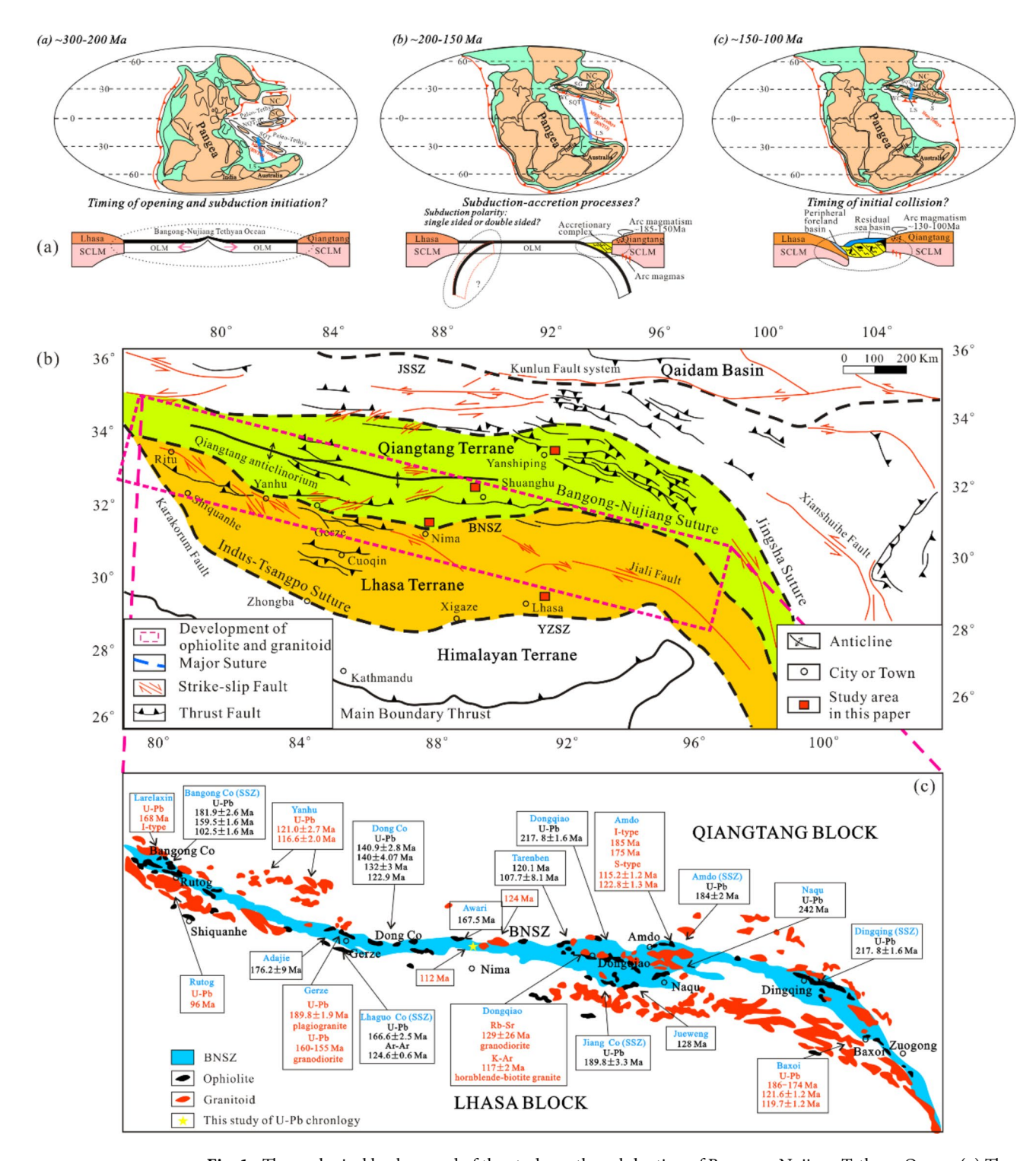


Fig. 1. The geological background of the study on the subduction of Bangong-Nujiang Tethyan Ocean. (a) The closed evolution process of the Bangong-Nujiang Tethyan Ocean (what is the subduction polarity and when is the initial collision). (b) Research on the tectonic framework of the Qinghai-Tibet Plateau and the Bangong-Nujiang suture zone (study area). (c) Zircon age of ophiolites and granitoids in the Bangong-Nujiang suture zone. JSSZ. Jingsha River suture zone, BNSZ. Bangong-Nujiang suture zone, YZSZ. Yarlung-Zangbo suture zone.

Block at 61 Ma. The Indian Continent collided with the southern Eurasia at 50 Ma, resulting in the complete closure of the Neo-Tethys Ocean³⁰. From north to south, the Qinghai-Tibet Plateau is divided into main tectonic units, such as the Songpan-Ganzi Terrane, the Qiangtang Block, the Lhasa Block and the Himalayan Orogenic Belt. The main tectonic blocks are connected by the Jinsha-River suture zone, the Bangong-Nujiang suture zone and the Yarlung-Zangbo suture zone, which are also traces of the demise of the Paleo and Neo-Tethys Oceans.

The Lhasa Block is a narrow shape from east to west, with a width of 150–300 km from north to south and a length of about 2500 km from east to west. Magmatic rocks are widely exposed, which is the most developed area of magmatism in the Tibetan Plateau (Fig. 2). The Lhasa Block is divided into three minor blocks from north to south: North Lhasa (NL), Central Lhasa (CL), and South Lhasa (SL) by the Shiquan River-Yongzhu-Namtso-Jiali Mixed Zone (SYMZ) and the Lobadui-Mira Mountain Fault Zone (LMF)³¹.

The Qiangtang Block is located between the Lhasa Block and the Songpan-Ganzi Terrane, bounded by the Jinsha-River suture zone on the north side and the Bangong-Nujiang suture zone on the south side, with a

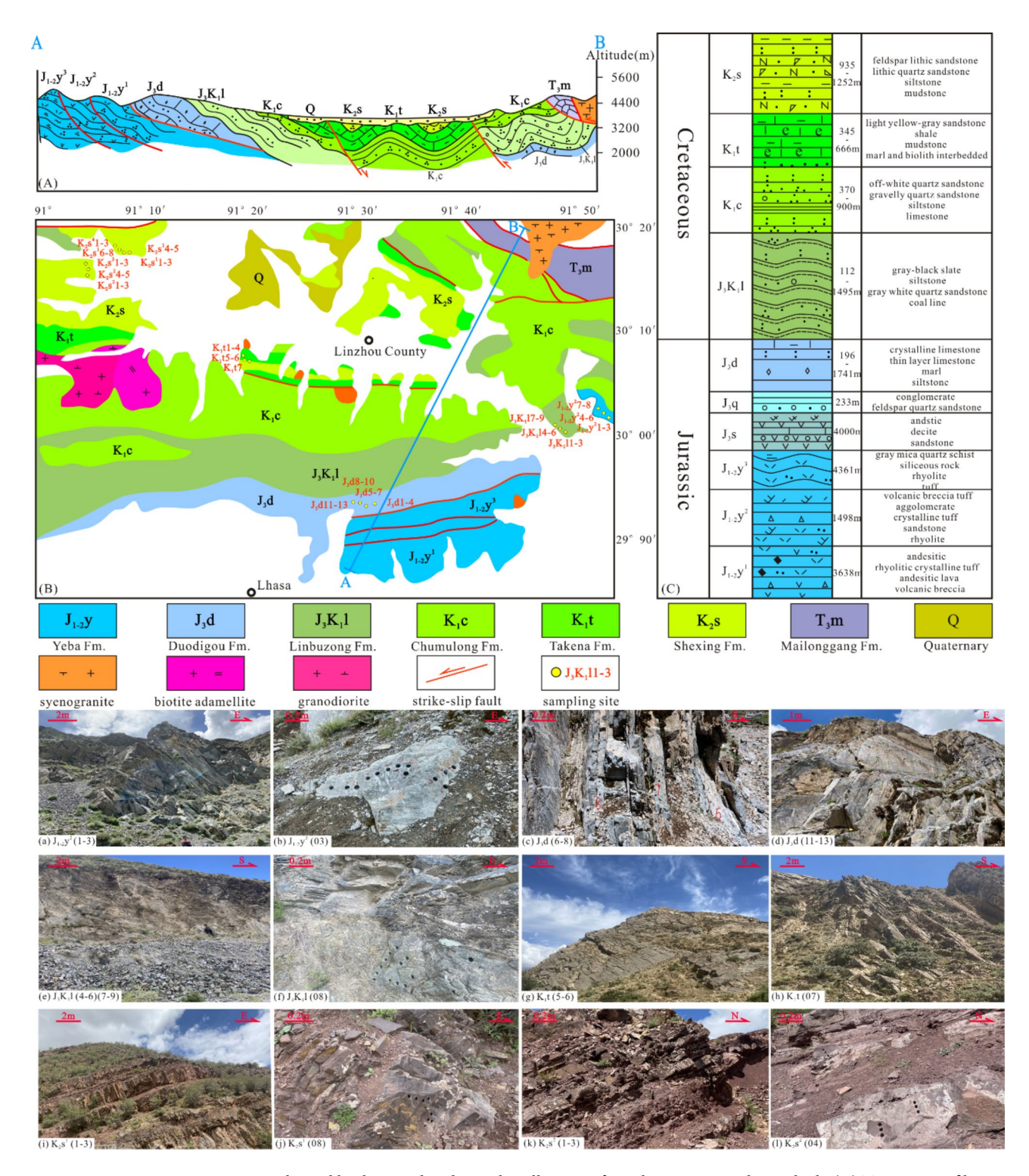


Fig. 2. Geological background and sample collection of Linzhou Basin in Lhasa Block. **(A)** Tectonic profile in the Linzhou Basin. **(B)** Geological background of the Linzhou Basin. **(C)** Lithological development of sedimentary strata in the Linzhou Basin. (a-l) Field outcrop photos of Linzhou Basin.

width of about 500–600 Km from north to south. The South and North Qiangtang Blocks are divided by the Longmuco-Shuanghu suture zone, which is mainly composed of the Central Uplift Zone (Fig. 3) and belongs to the Pan-African basement³². In the Late Paleozoic, marginal sea sedimentary structures developed, and in the Mesozoic, it evolved to the continental sea. The amalgamation history of the Qiangtang terrane involved the subduction, closure, and subsequent collision of the southern and northern Qiangtang blocks with the Paleo-Tethyan Ocean during the Late Triassic³³. Following this major tectonic event, the Qiangtang Block experienced complex deformation driven by multiple stress regimes: intracontinental extension and compression associated with the Songpan-Ganzi terrane³⁴; northward subduction of the Bangong-Nujiang Tethyan Ocean³⁵; and uplift of the central Qiangtang metamorphic belt³⁶.

The Bangong-Nujiang suture zone divides the Qiangtang Block on the north side and the Lhasa Block on the south side, representing the disappearance of Bangong-Nujiang Tethyan Ocean³⁷. The evolution process

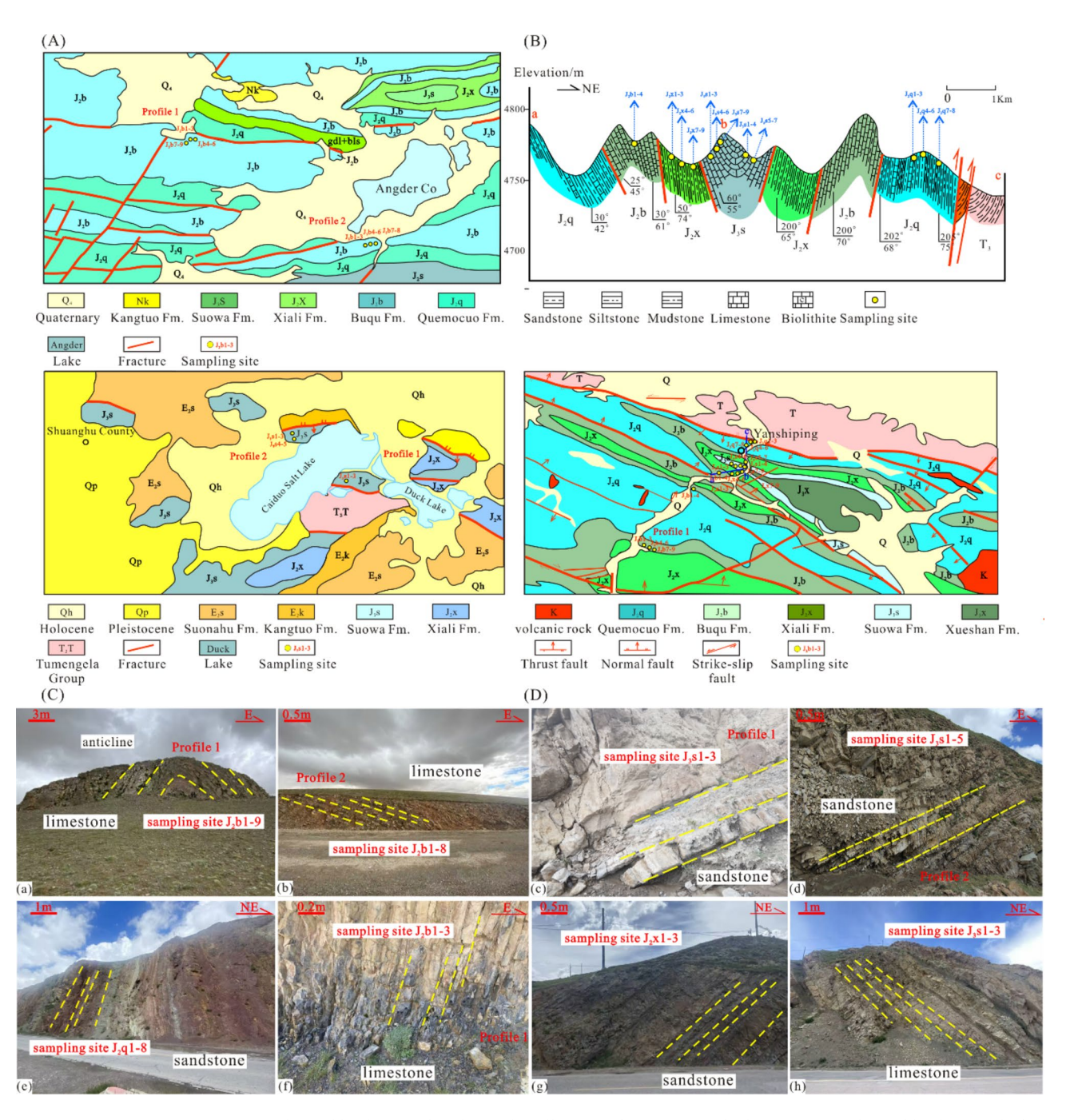


Fig. 3. Geological background and sample collection of Qiangtang Block. **(A) (C)** Geological background of the Shuanghu area in the Southern Qiangtang Block. **(D)** Geological background of the Yanshiping area in the Northern Qiangtang Block. **(B)** Tectonic profile of the Yanshiping area. (a-d) Field outcrop photos of Southern Qiangtang Block. (e-h) Field outcrop photos of North Qiangtang Block.

of the Bangong-Nujiang suture zone is complex, with continuous exposure of Jurassic ophiolites, accretionary complex, and intermediate-acidic magmatic rocks in the strata (Fig. 4). The suture zone and the widely developed magmatic rocks on both sides record the subduction and closure of the Bangong-Nujiang Ocean, as well as the collision between the Lhasa and Qiangtang Blocks. And the main sedimentary strata of the Bangong-Nujiang suture zone include the Mugagangri Group of the Early Middle Jurassic, the Shamulo Fm. of the Late Jurassic-Early Cretaceous, and overlying continental clastic rocks of the Late Cretaceous¹⁶.

Sample collection, experimentation and analysis methods

Sample collection

The samples for this study are widely distributed, including the Linzhou Basin in the Lhasa Block, the Shuanghu area and Yanshiping area in the Qiangtang Block, and the central area of the Bangong-Nujiang Suture Zone. Samples from the Linzhou Basin were collected from the Jurassic and Cretaceous strata. From bottom to top, 57 pyroclastic samples from the Middle Jurassic Yeba Fm. (J_2y) , 113 limestone samples from the Late Jurassic Duodigou Fm. (J_3d) , 74 siltstone samples from the Late Jurassic Linbuzong Fm. (J_3k_1l) , 33 sandstone samples interbedded with biogenic limestone from the Early Cretaceous Takena Fm. (K_1t) , and 179 red sandstone samples from the Late Cretaceous Shexing Fm. (K_2s) were collected. Moreover, 198 bioclastic and micrite limestone samples from the Middle Jurassic Buqu Fm. (J_3b) and 69 mudstone samples from the Late Jurassic Suowa Fm. (J_3s) were collected in the Shuanghu area of the Qiangtang Block. Clastic rocks from the Middle Jurassic Quemocuo Fm. (J_2q) , limestone from the Middle Jurassic Buqu Fm. (J_3s) were collected in the Yanshiping area of the Qiangtang Block. In addition, 231 red sandstone samples from the Late Cretaceous Jingzhushan Fm. (K_2j) were collected on the south side of the Bangong-Nujiang suture zone, and 34 sandstone samples from the Late Jurassic Shamulo Fm. (J_3s) and 36 volcanic breccia samples were collected inside the Bangong-Nujiang suture zone.

Experimentation

Cylindrical specimens measuring 25 mm in diameter and 22 mm in height were prepared for AMS measurements, which were conducted at the State Key Laboratory of Continental Dynamics, Northwest University. The AMS analysis was performed using the AGICO MFK1-FB Kappabridge system (Czech Republic) operating at a field strength of 300 $\text{A}\cdot\text{m}^{-1}$, with a detection limit of $2\times10^{-8}\text{SI}$ and measurement accuracy of 1%. The acquired data were processed and analyzed using Anisoft 4.2 software, with the detailed results presented in Table 1.

Zircon U-Pb geochronological analyses were conducted at Nanjing Hongchuang Geological Survey Technical Services Co., Ltd. Zircon grains exhibiting well-defined oscillatory zoning and intact crystal morphology were carefully selected for analysis, with particular attention to avoid fractures and mineral inclusions. The analytical procedure involved multiple steps, including signal selection for samples and blanks, instrumental drift correction, elemental concentration determination, and U-Th-Pb isotopic ratio calculation. For quality control and isotopic fractionation correction, international reference materials including zircon standard 91,500 and GJ-1 (Australia) were routinely analyzed as external standards throughout the U-Pb dating process.

Analysis of stress and magnetic fabric characteristics

The dynamics of oceanic crust subduction are primarily governed by three fundamental mechanisms: the migration of oceanic ridges, the slab pull force of subducting plates, and the basal drag of oceanic plates³⁹. Among these forces, the initial plate motion is mainly driven by slab sliding, while the dominant driving force during subduction is the slab pull force. When a continental block experiences oceanic plate subduction, it is subjected to compressive stress that aligns with the motion direction of the subducting oceanic plate. Following ocean closure, the relative motion between continental blocks is controlled by the resultant stress field, which represents the vector difference between the paleostress and the minimum compressive stress directions. In this post-collisional stage, the absence of oceanic subduction-induced compressive stress leads to a tectonic regime where the local motion between continental blocks is primarily driven by mantle-derived magmatic drag forces.

In magnetic fabric analysis, a direct correlation between specific fabric typesand all measured samples cannot be universally established¹⁷. To address this limitation, the study employs a systematic approach by correlating magnetic lineation with structural features including pencil-like and tensile lineation, while associating magnetic foliation with deformation characteristics ranging from initial deformation to weak and strong cleavage development. The analytical procedure involves the application of F-Linn diagrams to differentiate samples dominated by magnetic foliation from those exhibiting prominent magnetic lineation. Subsequently, the fabric types are determined through comprehensive analysis of magnetic susceptibility ellipsoid distribution patterns at each sampling site, enabling detailed characterization of individual specimens.

Test results Zircon U-Pb geochronology

For zircon U-Pb geochronological analysis, clastic rocks of the Shamuluo Fm. within the Bangong-Nujiang suture zone were systematically sampled. The zircon population exhibits a color spectrum ranging from off-white to yellowish, with occasional light reddish hues. Zircon morphology varies from euhedral to subhedral, with some grains displaying irregular shapes due to fragmentation. Sandstone-hosted zircons typically exhibit ellipsoidal to short-prismatic forms, with well-preserved grains measuring approximately 100 µm along the long axis and 30–50 µm along the short axis (Fig. 5b). In contrast, zircon from volcaniclastic rocks displayed more elongated prismatic morphologies, with maximum long axis dimensions reaching 200 µm (Fig. 5d). The majority of zircons exhibit well-defined oscillatory zoning, particularly pronounced in volcaniclastic samples. A

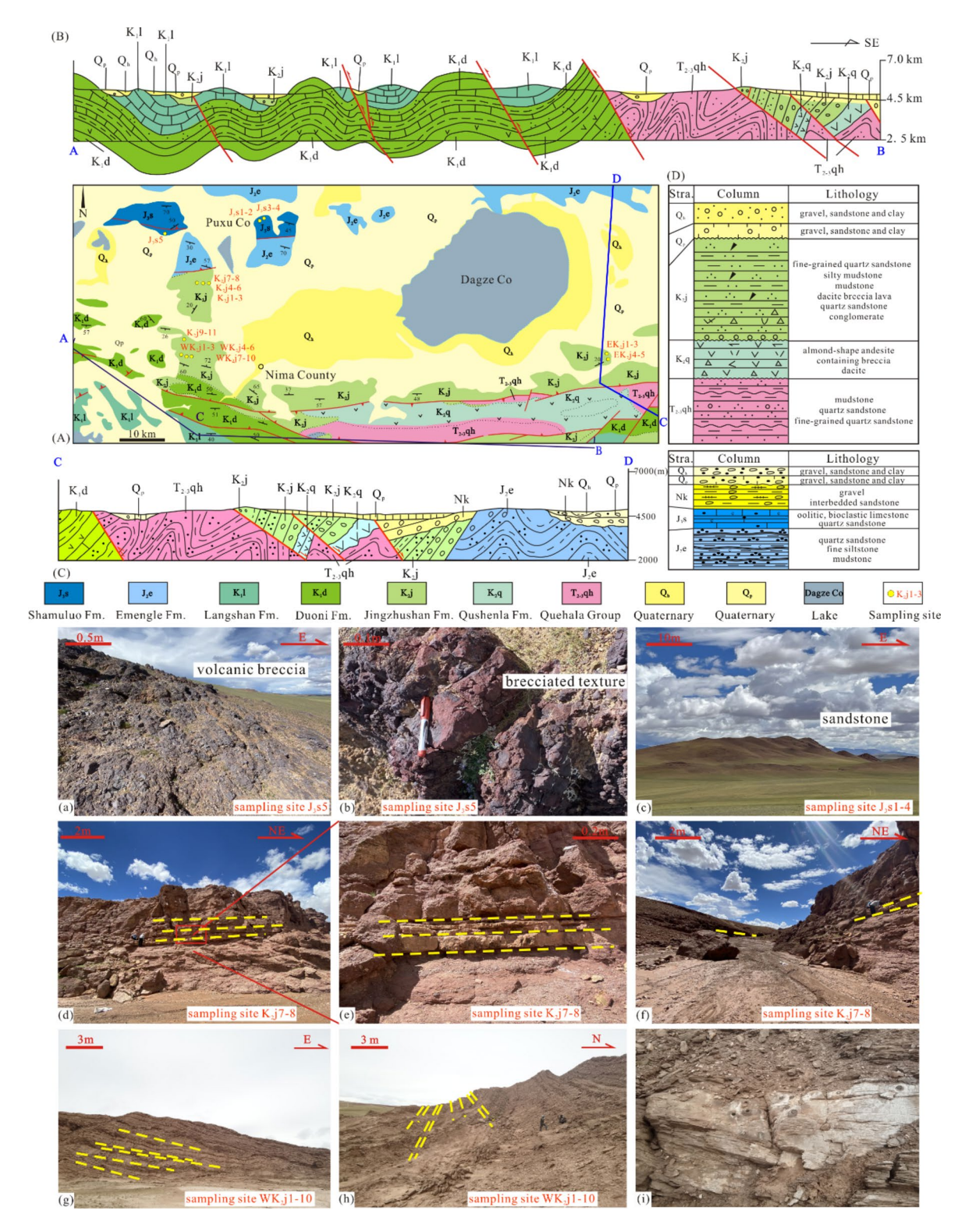


Fig. 4. Geological background and sample collection of Bangong-Nujiang suture zone. **(A)** Geological background of the Nyima Basin. **(B) (C)** Tectonic profiles of the Nyima Basin. **(D)** Lithological development of sedimentary strata of the Nyima Basin. (a-i) Field outcrop photos of Nyima Basin in the Bangong-Nujiang suture zone $((d-i)^{38})$.

Samples	N	Km	L	F	Pj	Т	K1	K2	К3
Linzhou Basin, Lhasa Block									
J ₂ Y	59	429×10^{-6}	1.058	1.056	1.119	-0.090	33.2/11.9	126.3/14.2	264.7/71.3
J ₃ D	106	-5.82×10^{-6}	1.060	1.060	1.129	-0.003	247.2/27.6	155.3/3.7	58.2/62.1
J ₃ K ₁ L	66	1600×10 ⁻⁶	1.010	1.019	1.031	0.416	184.5/3.1	94.2/6.0	301.9/83.3
K ₁ T	32	67.9×10^{-6}	1.008	1.006	1.014	-0.086	340.5/68.7	89.1/7.1	181.7/20.0
K2S (1)	71	309×10^{-6}	1.025	1.029	1.055	0.055	301.2/3.1	33.6/37.7	207.3/52.2
K2S (2)	50	147×10^{-6}	1.007	1.007	1.015	-0.122	105.0/1.3	196.5/48.6	13.8/41.4
K2S (3)	25	68.8×10 ⁻⁶	1.007	1.008	1.015	0.089	318.9/1.1	228.7/13.5	53.4/76.5
K2S (4)	33	218×10^{-6}	1.023	1.030	1.054	0.119	307.0/5.9	45.0/53.4	212.7/35.9
Yanshiping area, Northern Qiangtang Block									
J ₂ Q	66	182×10 ⁻⁶	1.009	1.011	1.021	0.040	207.5/4.5	328.8/81.3	116.9/7.4
J ₂ B (1)	33	354×10^{-6}	1.008	1.009	1.017	0.113	111.9/50.0	203.1/1.0	293.9/40.0
J ₂ B (2)	64	655×10 ⁻⁶	1.017	1.030	1.049	0.250	158.6/32.8	285.5/42.9	47.2/29.5
J ₂ B (3)	25	1220×10^{-6}	1.022	1.018	1.041	-0.111	298.9/36.3	97.8/51.7	201.2/10.3
J ₂ X	66	159×10^{-6}	1.011	1.012	1.024	0.018	250.4/2.6	159.8/12.7	351.8/77.0
J ₃ S (1)	65	132×10^{-6}	1.006	1.006	1.013	-0.012	348/30.1	149.4/58.5	253.3/8.4
J ₃ S (2)	72	174×10 ⁻⁶	1.007	1.009	1.016	0.075	247.0/0.3	156.9/12.5	338.5/77.5
Shuanghu area, Southern Qiangtang Block									
J ₂ B (1)	74	67.2×10 ⁻⁶	1.012	1.029	1.044	0.331	57.3/77.4	263.1/11.4	172.0/5.3
J ₂ B (2)	87	34.2×10^{-6}	1.014	1.048	1.066	0.474	179.1/78.6	61.2/5.4	330.3/10.0
J ₃ A (1)	25	67.4×10 ⁻⁶	1.020	1.004	1.026	-0.386	88.9/77.3	274.9/12.6	184.6/1.3
J ₃ A (2)	42	32.7×10^{-6}	1.004	1.006	1.010	0.149	341.5/21.9	-242.5/21.3	112.8/58.7
Bangong-Nujiang suture zone									
J ₃ S	34	135×10^{-6}	1.002	1.003	1.005	0.277	265.5/5.2	356.0/6.2	135.7/81.9
K ₂ J (1)	39	155×10 ⁻⁶	1.008	1.002	1.011	-0.463	32.3/7.9	137.6/62.3	298.4/26.4
K ₂ J (2)	28	234×10^{-6}	1.007	1.025	1.031	0.402	120.1/8.2	24.5/34.1	221.8/54.6
K ₂ J (3)	92	372×10 ⁻⁶	1.010	1.022	1.033	0.344	288.4/0.7	18.5/8.3	193.6/81.7

Table 1. AMS parameters of Jurassic-Cretaceous sedimentary strata in the central Tibetan plateau measured at room temperature.

minor population of zircons displays distinct core-rim structures, characterized by oscillatory-zoned cores and homogeneous, gray-white rims lacking internal zoning.

Zircon U-Pb geochronological analysis revealed distinct age distributions between detrital sandstones and volcaniclastic rocks. Detrital sandstones yielded zircon ages ranging from 112 Ma (youngest) to 2584 Ma (oldest), while volcaniclastic rocks showed a younger age range from 95 Ma to 2760 Ma. The detrital zircon population displays seven prominent age peaks at 131-112 Ma, 380-213 Ma, 480-415 Ma, 840-627 Ma, 987-902 Ma, 1923-1816 Ma, and 2584-2417 Ma, respectively (Fig. 5a). In contrast, volcaniclastic zircons exhibit a single dominant age peak between 116 and 95 Ma, with a weighted mean age of 102.9 ± 0.9 Ma (Fig. 5c). Age distribution analysis indicates that detrital zircons are predominantly concentrated in the 500-100 Ma (60–70%), followed by 1000-600 Ma (20–25%), with minor populations in the 2000-1800 Ma and 2500 Ma (5–10%). Volcaniclastic zircons, however, show a markedly different distribution pattern, with > 90% of grains clustering within the 120-90 Ma interval.

Anisotropy of magnetic susceptibility

Linzhou basin of Lhasa block

The Middle Jurassic Yeba Fm. (J_2y) demonstrates a mean magnetic susceptibility (Km) value of 429×10^{-6} SI, indicating significantly enhanced magnetic properties characteristic. The mean anisotropy degree (Pj) of 1.119 suggests the presence of weaktectonic strain (Fig. 6(b) (c)). The magnetic lineation, as indicated by the orientation of the maximum susceptibility axis (Kmax), reveals a SW-NE trending paleostress direction, whereas the minimum susceptibility axis (Kmin) orientation corresponds to the SWW-NEE direction of the maximum compressive stress (Fig. 6a). The magnetic susceptibility ellipsoid characteristics suggest that the Yeba Fm. experienced alternating extensional and compressional tectonic conditions, with corresponding magnetic fabric types ranging from initial deformation through pencil-like to tensile lineation.

The Late Jurassic Duodigou Fm. (J₃d) exhibits a Km ranging from -8.51 to 3.17×10^{-6} SI, with a Pj of 1.743, suggesting significant tectonic strain (Fig. 6(e) (f)). Magnetic fabric analysis reveals that the Kmax orientation indicates a NEE-SWW trending paleostress direction, while the Kmin orientation corresponds to the SSE-NNW direction of maximum compressional stress (Fig. 6d). The magnetic susceptibility ellipsoid characteristics demonstrate that the Duodigou Fm. developed under predominantly compressional tectonic conditions, exhibiting magnetic fabric types characteristic of both initial deformation and pencil-like.

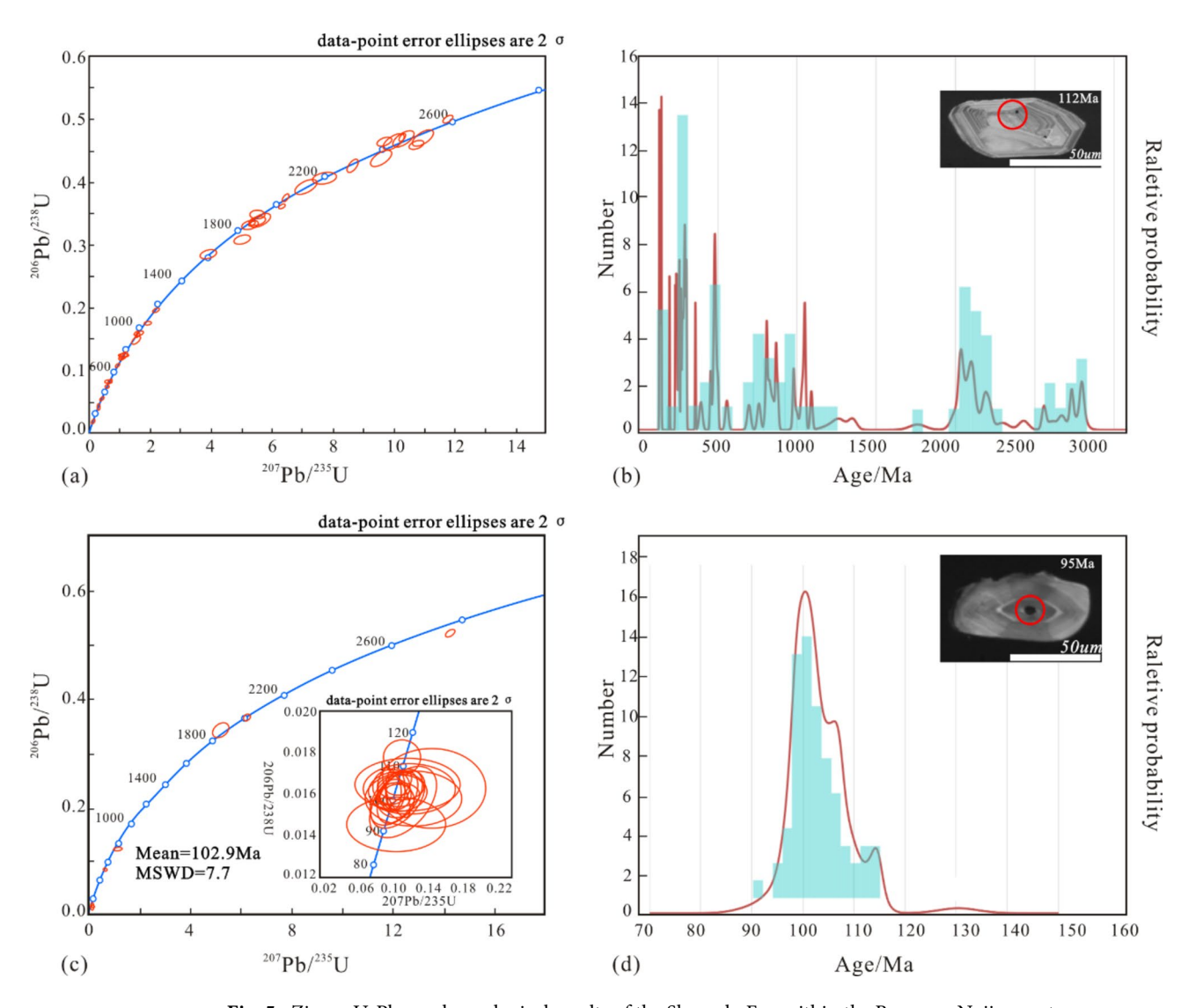


Fig. 5. Zircon U-Pb geochronological results of the Shamulo Fm. within the Bangong-Nujiang suture zone. (a) Concordia diagram showing U-Pb ages of detrital zircons from sedimentary clastic rocks. (b) Probability density plot of detrital zircon ages from sedimentary clastic rocks. (c) Concordia diagram displaying U-Pb ages of zircons from volcaniclastic rocks. (d) Probability density plot of zircon age distribution from volcaniclastic rocks.

The Late Jurassic Linbuzong Fm. (J_3k_1l) displays a Km of 1600×10^{-6} SI, with a Pj of 1.031, suggesting minimal tectonic strain (Fig. 6(h) (i)). Magnetic fabric analysis reveals that the formation developed under compressional tectonic conditions, as evidenced by the presence of sedimentary fabric, initial deformation fabric, and pencillike fabric in the magnetic susceptibility ellipsoid characteristics (Fig. 6g).

The Early Cretaceous Takena Fm. (K_1) exhibits a Km of 67.9×10^{-6} SI. Magnetic fabric analysis indicates that the Kmax orientation shows SSE-NNW trending paleostress direction, while the Kmin orientation corresponds to the N-S direction of maximum compressive stress (Fig. 6j). The magnetic susceptibility ellipsoid characteristics demonstrate that the Takena Fm. developed under extensional tectonic conditions, displaying magnetic fabrics including strong cleavage and tensile lineation (Fig. 6(k) (l)).

The Late Cretaceous Shexing Fm. (K_2S) displays a range of Km values from 309 to $68.8 \times 10^{-6}SI$ across four measured profiles. Anisotropy analysis reveals distinct strain patterns, with profile 1 and profile 4 showing a same Pj of 1.055, while profile 2 and profile 3 exhibit lower values of 1.015. Paleostress orientations, as indicated by the Kmax, show SE-NW trend in profile 1, profile 3, and profile 4, contrasting with NWW-SEE orientation in profile 2. The Kmin orientations demonstrate varying compressive stress directions: profiles 1 and 4 show NE-SW maximum compressional stress directions (Fig. 6(m) (v)), while profile 2 and profile 3 exhibit SWW-NEE and SW-NE directions, respectively (Fig. 6(p) (s)). Magnetic susceptibility ellipsoid characteristics suggest that the Shexing Fm. experienced both compressional and extensional tectonic conditions. Magnetic fabric analysis indicates that profiles 1, 3, and 4 are characterized by initial deformation and pencil-like (Fig. 6(n) (o) (t) (u) (w) (x)), whereas profile 2 displays pencil-like fabric and strong cleavage fabric (Fig. 6(q) (r)).

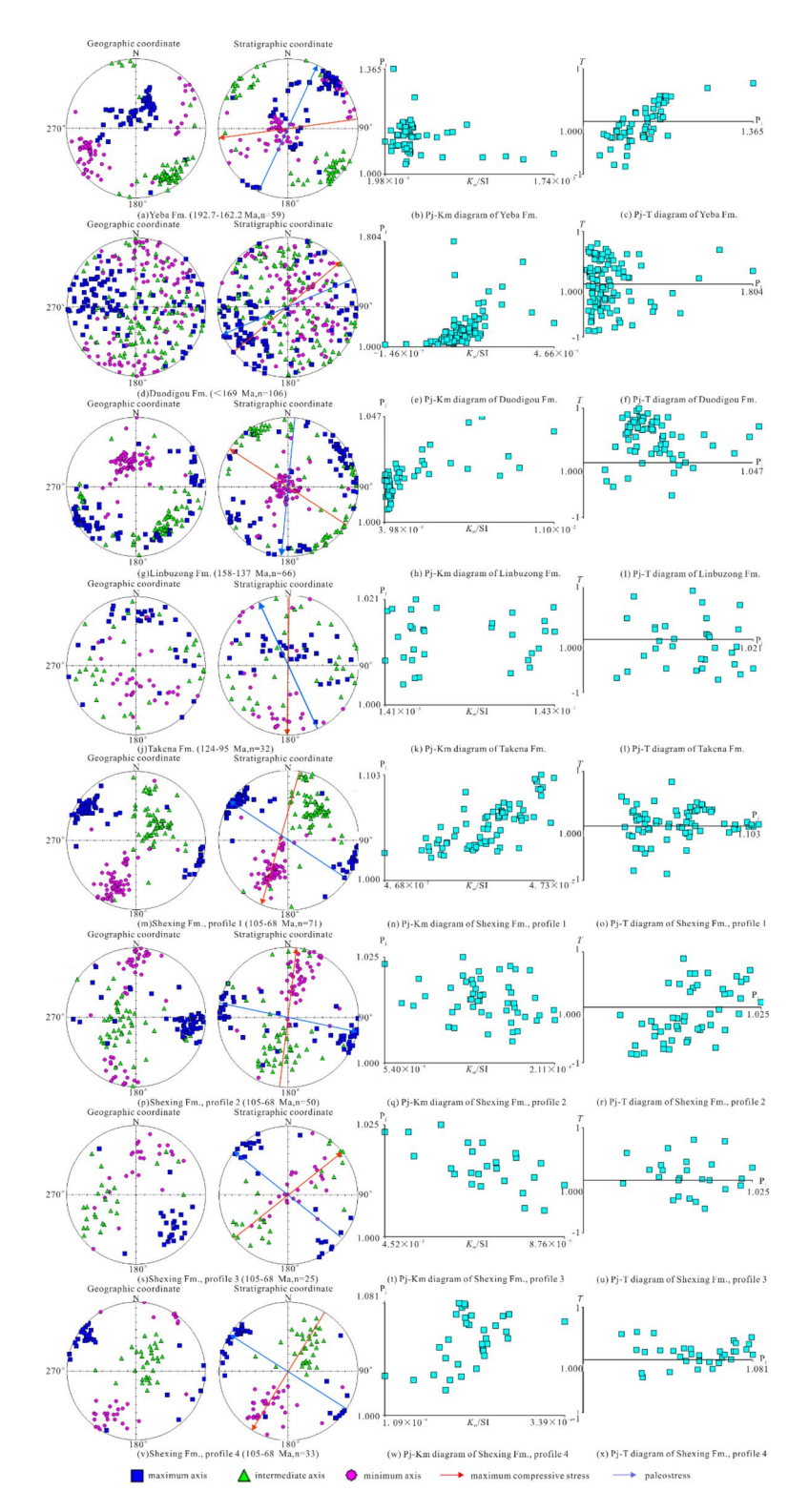


Fig. 6. AMS characteristics of various stratigraphic units in the Linzhou Basin, Lhasa Block.

Qiangtang block

Yanshiping area

The Middle Jurassic Quemocuo Fm. (J_2q) in the Yanshiping area exhibits a Km of 182×10^{-6} SI and a Pj of 1.021. Magnetic fabric orientation analysis reveals that the Kmax indicates a NE-SW trending paleostress direction, while the Kmin orientation corresponds to the NW-SE direction of maximum compressional stress (Fig. 7a). The magnetic susceptibility ellipsoid characteristics demonstrate that the Quemocuo Fm. experienced alternating

extensional and compressional tectonic conditions, as evidenced by the development of diverse magnetic fabrics including initial deformation, pencil-like, and both weak and strong cleavage fabrics (Fig. 7(b) (c)).

The Middle Jurassic Buqu Fm. (J2b) displays distinct Km values across three measured profiles, with mean values of 354, 655, and 1220×10^{-6} SI, respectively. Corresponding Pj shows progressive strain variation, measuring 1.017, 1.049, and 1.041 for each profile. Magnetic fabric orientation analysis reveals that the Kmax orientations indicate NW-SE trending paleostress directions in profiles 1 and 2, contrasting with SEE-NWW orientation in profile 3. The Kmin orientations demonstrate varying maximum compressive stress directions:

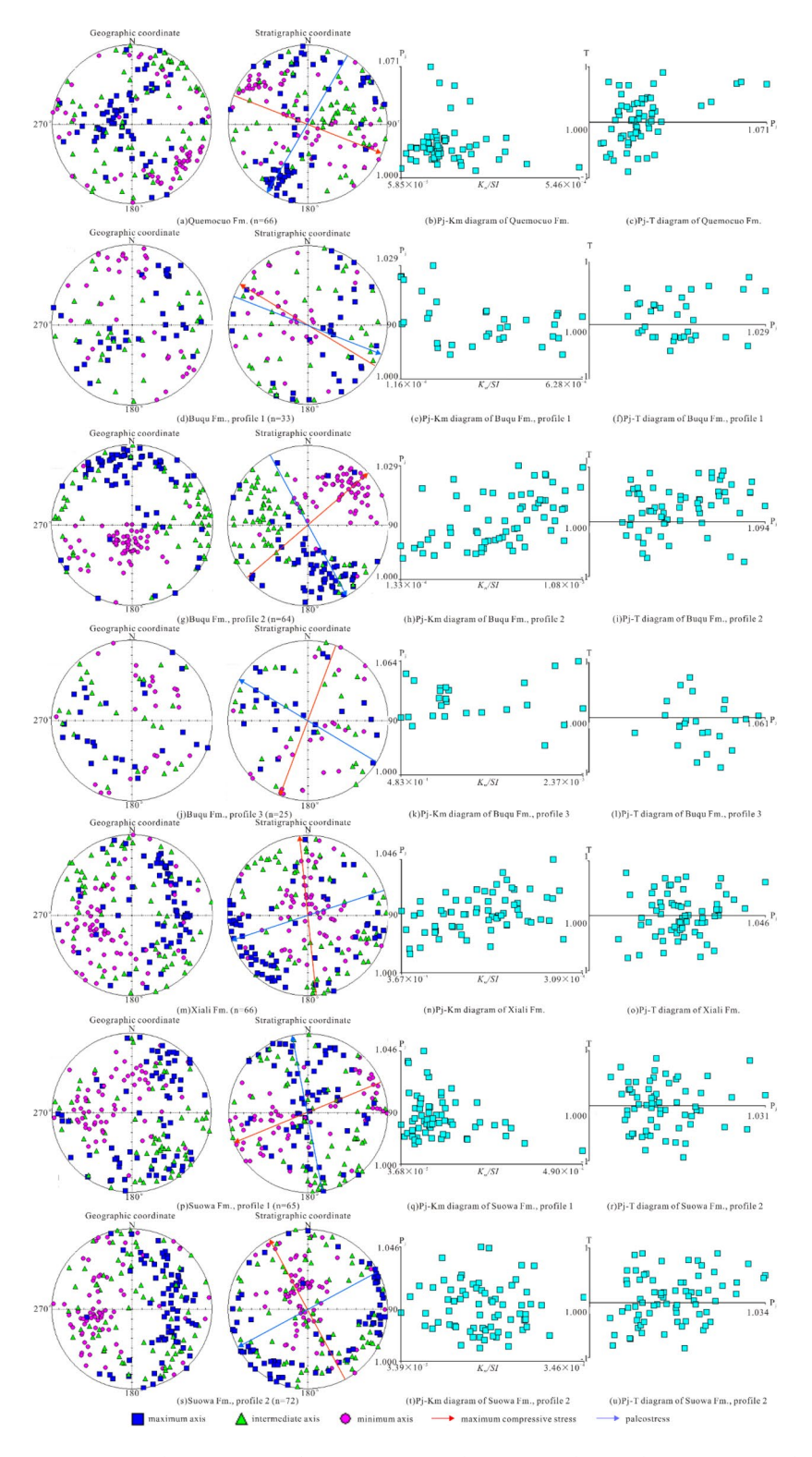


Fig. 7. AMS characteristics of various stratigraphic units in the Yanshiping area, Northern Qiangtang Block.

SEE-NWW in profile 1 (Fig. 7d), SW-NE in profile 2 (Fig. 7g), and NE-SW in profile 3(Fig. 7j). Magnetic susceptibility ellipsoid characteristics suggest that the Buqu Fm. experienced complex tectonic conditions, alternating between extensional and compressional conditions, as evidenced by the development of diverse magnetic fabrics including initial deformation, pencil-like (Fig. 7(e) (f)), strong cleavage (Fig. 7(h) (i)), and tensile lineation (Fig. 7(k) (l)).

The Middle Jurassic Xiali Fm. (J_2x) exhibits a Km of 159×10^{-6} SI and a Pj of 1.024. Magnetic fabric orientation analysis reveals that the Kmax indicates a NE-SW trending paleostress direction, while the Kmin orientation corresponds to the S-N direction of maximum compressional stress (Fig. 7m). The magnetic susceptibility ellipsoid characteristics demonstrate that the Xiali Fm. developed under a transitional tectonic condition, with predominant extensional features. This tectonic condition is evidenced by the development of characteristic magnetic fabrics, including initial deformation, pencil-like, and strong cleavage (Fig. 7(n) (o)).

The Late Jurassic Suowa Fm. (J3s) displays distinct Km values of 132 and 174×10^{-6} SI across two measured profiles, with corresponding Pj values of 1.013 and 1.016, respectively. Magnetic fabric analysis reveals contrasting paleostress orientations: in profile 1, the Kmax orientation indicates SSE-NNW trending magnetic lineation, corresponding to the paleostress direction, while the Kmin shows NEE-SWW orientation of maximum compressive stress (Fig. 7p). Profile 2 exhibits different orientations, with Kmax indicating NE-SW trending magnetic lineation and Kmin corresponding to SSE-NNW maximum compressive stress direction (Fig. 7s). The magnetic susceptibility ellipsoid characteristics demonstrate that the Suowa Fm. developed under a transitional tectonic condition, as evidenced by the presence of diverse magnetic fabrics including initial deformation, pencil-like (Fig. 7(t) (u)), strong cleavage, and tensile lineation (Fig. 7(q) (r)).

Shuanghu area

The Middle Jurassic Buqu Fm. (J2b) exhibits distinct Km values across two profiles, measuring 67.2 and 34.2×10^{-6} SI, respectively, with corresponding Pj values of 1.044 and 1.066. Magnetic fabric orientation analysis reveals contrasting stress orientations: in profile 1, the Kmax orientation indicates SW-NE trending magnetic lineation, corresponding to the paleostress direction, while the Kmin shows NW-SE maximum compressive stress (Fig. 8a). Profile 2 displays different orientations, with Kmax indicating N-S trending magnetic lineation and Kmin corresponding to SE-NW oriented compressive stress (Fig. 8d). The magnetic susceptibility ellipsoid characteristics demonstrate that the Buqu Fm. developed under predominantly extensional tectonic conditions, as evidenced by the development of strong cleavage fabric and tensile lineation fabric (Fig. 8(b) (c) (e) (f)).

The Late Jurassic Suowa Fm. (J_3S) displays distinct Km values across two profiles, measuring 67.4 and 32.7×10^{-6} SI, respectively, with corresponding Pj values of 1.026 and 1.010. Magnetic fabric orientation analysis reveals contrasting tectonic conditions: in profile 1, the Kmax orientation indicates SW-NE trending magnetic lineation, corresponding to the paleostress direction, while the Kmin shows NE-SE oriented maximum compressive stress (Fig. 8g). Profile 2 exhibits different stress patterns, with Kmax indicating SSE-NNW trending paleostress and Kmin corresponding to NWW-SEE oriented compressive stress (Fig. 8j). Magnetic susceptibility ellipsoid characteristics demonstrate distinct tectonic conditions: profile 1 indicates extensional condition, characterized by strong cleavage fabric and tensile lineation fabric (Fig. 8(h) (i)), while profile 2 reflects compressional condition, evidenced by initial deformation fabric and pencil-like fabric (Fig. 8(k) (l)).

Bangong-Nujiang suture zone

The Shamulo Fm. (J_3S) within the Bangong-Nujiang suture zone exhibits a Km value of $1.35 \times 10^{-6}SI$ and a Pj value of 1.005.Magnetic fabric analysis reveals a dispersed orientation pattern, with the Kmax showing no preferred orientation within the ellipsoid. In contrast, the Kmin displays a central concentration in the ellipsoid, suggesting NW-SE oriented maximum compressional stress with minimal strain development (Fig. 9a). The magnetic fabric is predominantly characterized by sedimentary and initial deformation, with rare occurrences of pencil-like fabric (Fig. 9(b) (c)). These magnetic susceptibility ellipsoid characteristics indicate that the Shamulo Fm. developed under extensional tectonic condition.

Furthermore, the Late Cretaceous Jingzhushan Fm. (K_2j) within the Bangong-Nujiang suture zone displays a progressive increase in Km values, measuring 155, 194, 234, and 372×10^{-6} SI, respectively. Correspondingly, the Pj show values of 1.011, 1.038, 1.033, and 1.033. Magnetic fabric analysis reveals that only one profile exhibits distinct tectonic features (Fig. 9(e) (f)), with the Kmax orientation indicating NE-SW trending paleostress and the Kmin showing NW-SE oriented maximum compressive stress, accompanied by pencil-like fabric (Fig. 9(d) (h) (k)). In contrast, samples from the remaining profiles predominantly exhibit sedimentary magnetic fabric (Fig. 9(i) (g) (l) (m)), as evidenced by their magnetic susceptibility ellipsoid characteristics.

Discussions

Sequence of deposition time in the middle Jurassic-Late cretaceous

Based on this study and existing chronological data, the depositional timing of Middle Jurassic to Late Cretaceous strata in the Central Tibetan Plateau has been systematically determined. This chronological framework enables precise comparison of tectonic stresses across different regions during the same period, thereby providing critical constraints for reconstructing the closure process of the Bangong-Nujiang Tethyan Ocean (Fig. 10).

Chronological studies were conducted on volcanic rocks such as basalt and rhyolite from the Yeba Fm. of the Linzhou Basin in the Lhasa Block, obtaining stratigraphic ages of 176.9 ± 2.3 Ma, 162.2 ± 3.3 Ma 40 , 181 ± 5.0 Ma, 181.4 ± 4.4 Ma, 192.7 ± 1.3 Ma, and 188.8 ± 1.8 Ma 41 , respectively. At present, there is relatively little research on the chronology of the Duodigou Fm. Chronological research was conducted on the underlying Quesangwenquan Fm. of the Duodigou Fm., and the youngest zircon age of 169 Ma from the quartz sandstone was obtained the chronological study of detrital zircons and volcanic interlayers in the Linbuzong Fm. indicates that the stratigraphic age ranges from 158 ± 1.2 Ma to 137 ± 2 Ma. It is believed that the bottom dwelling foraminifera of

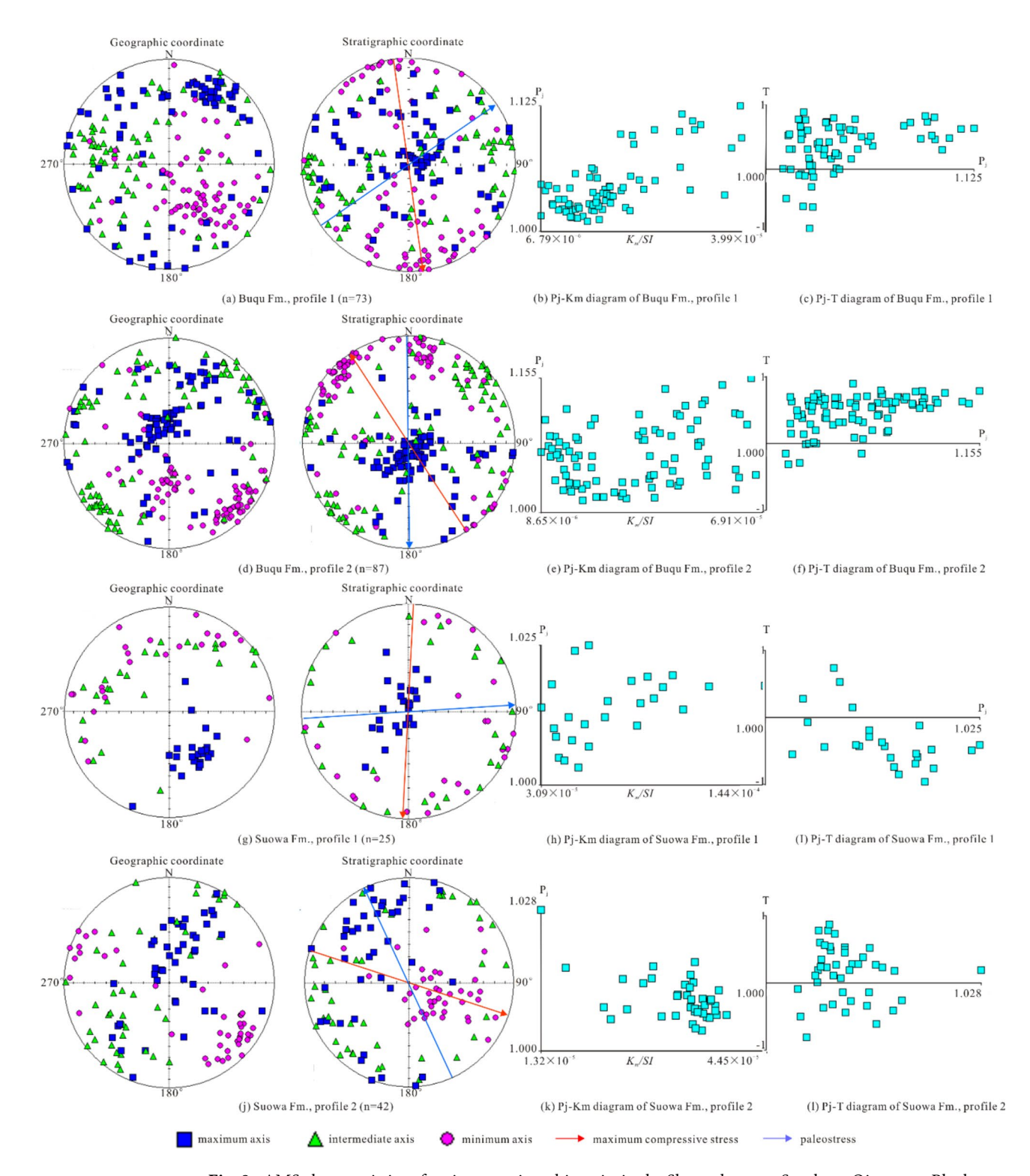


Fig. 8. AMS characteristics of various stratigraphic units in the Shuanghu area, Southern Qiangtang Block.

the Takena Fm. lived among 124-119 Ma (Middle Aptian stage)⁴³ by the fossil identification. The stratigraphic ages obtained from the Shexing Fm. are concentrated at 98-68Ma⁴⁴.

The Buqu Fm. in the Qiangtang Block is generally believed to have been deposited during the period of Bathonian-Early Callovian in the Middle Jurassic, and may have also entered the Bajocian Stage⁴⁵. The Quemocuo Fm. had unconformable contact with the underlying Nadigangri Fm., and had conformable contact with the overlying Buqu Fm. Previous studies on the chronology of the Nadigangri Fm. suggest a deposition age of 209-197Ma⁴⁶. The Xiali Fm. developed detrital rocks and was integrated contact with both the underlying Buqu Fm. and the overlying Suowa Fm⁴⁷. Fossil and climatic research on the lower part of the Suowa Fm. indicate that it

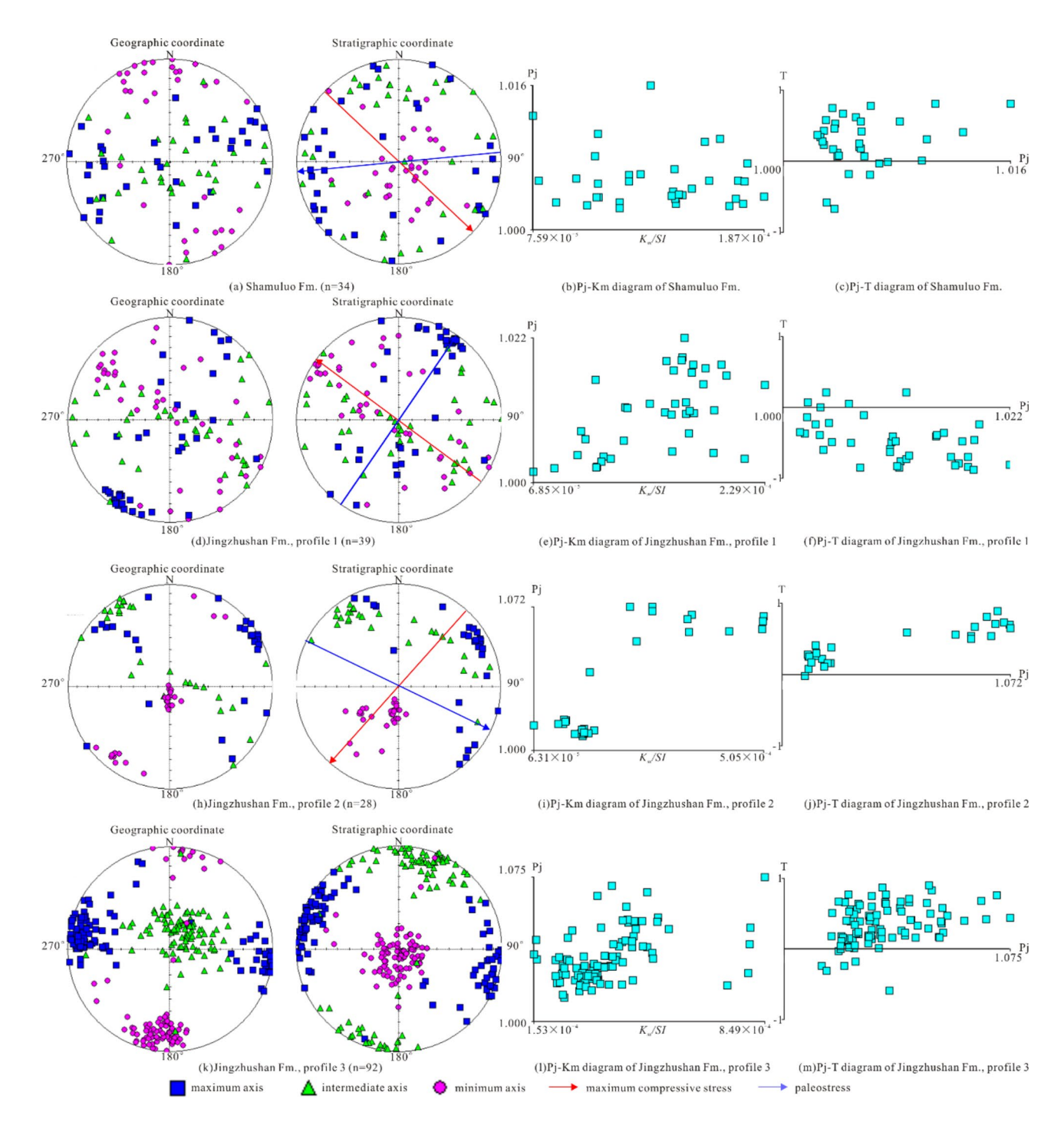


Fig. 9. AMS characteristics of various stratigraphic units in the Nyima Basin, Bangong-Nujiang suture zone.

belongs to the Oxfordian Stage, with an age among 163.5-157.3Ma⁴⁸. In addition, some studies suggest that the upper part of the Suowa Fm. belong to the period of Late Jurassic-Early Cretaceous⁴⁹.

The Shamulo Fm. in the Bangong-Nujiang suture zone developed shallow marine strata⁵⁰, and granite porphyry with zircon ages of 151 ± 2 Ma were obtained from siliceous clastic-carbonate sediments in the North Nyima County, deposited from the Oxfordian Stage to the Kimmerian Stage⁵¹. The zircon ages from the volcanic rocks of the Lower Shamulo Fm. in the Geji area are 141 Ma and 134 Ma, while the oldest zircon age from the Upper Shamulo Fm. is 101 Ma, belonging to the Albian Stage⁵². The weighted age of the volcanic rocks from the Shamulo Fm. obtained in this study is 102.9 Ma, with the youngest zircon age of 95 Ma, and the youngest zircon age obtained from detrital sandstone is 112 Ma. At the same time, there may be a diachroneity coincidence between the Shamulo Fm. and the Suowa Fm., such as the granodiorite vein at 151 ± 2 Ma that invaded the Shamulo Fm. and the clastic rocks of the Shamulo Fm. at 143 Ma and 163Ma⁵³. However, based on the age of the Shamulo Fm. in this paper, it can be considered that the deposition time of the Suowa Fm. was earlier

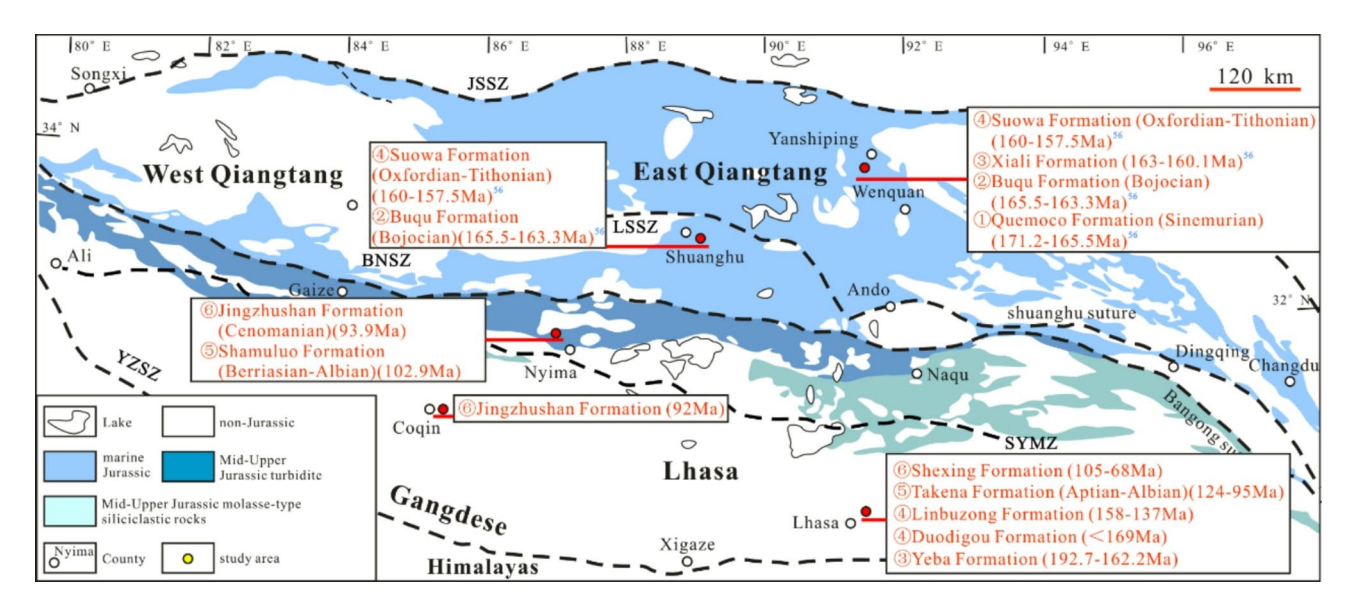


Fig. 10. Study on the deposition sequence of strata from the Middle Jurassic to the Late Cretaceous. JSSZ. Jingsha River suture zone, LSSZ. Longmuco-Shuanghu suture zone, BNSZ. Bangong-Nujiang suture zone, SYMZ. Shiquan River-Yongzhu-Namtso suture zone, YZSZ. Yarlung-Zangbo suture zone. (Identical sequence numbers demonstrate stratigraphic synchroneity across different study areas, indicating contemporaneous depositional periods. A representative example is the temporal equivalence between the Takena Fm. and Shexing Fm. in the Linzhou Basin with the Shamulo Fm. and Jingzhushan Fm. in the Nyima Basin, respectively.)

than that of the Shamulo Fm. The ages obtained from the Jingzhushan Fm. in the Bangong-Nujiang suture zone include 96 Ma (Cenomanian Stage of the Late Cretaceous) 37 , 89 ± 0.66 Ma, 102.7 ± 1.4 Ma, and 100-73Ma 54,55 .

Stress analysis during the same deposition time

Early middle jurassic

The research strata on the early stage of Middle Jurassic include the early Buqu Fm. in the Shuanghu area of the Qiangtang Block, Quemoco Fm. and early Buqu Fm. in the Yanshiping area of the Qiangtang Block. Based on the stress analysis, the Shuanghu area is considered to be the center of tectonic activity at this time, and is considered to be caused by the northward subduction of the Bangong-Nujiang Tethyan Ocean, which generates northward compressive stress. The tectonic activity experienced by the Yanshiping area is related to the southward extension of the Songpan-Ganzi Terrane, represented as southward compression. This activity is related to the continuation of the Indosinian Movement in the Early-Middle Jurassic and the western response of the Yanshan Movement. At the same time, the direction of stress decomposition may represent the mantle's dragging effect on the plate. Due to the deposition time of the Quemoco Fm. being slightly earlier than that of the Buqu Fm., the mantle simultaneously exerted counterclockwise and clockwise drag on the Shuanghu area and Yanshiping area (Fig. 11). This dragging situation may be the main reason for a strong expansion and subsidence process that occurred in the Qiangtang Block during the early stage of Middle Jurassic.

Late middle jurassic

The research strata on the late stage of Middle Jurassic include the Yeba Fm. in the South Lhasa Block, the Late Buqu Fm. in the Shuanghu area of the Qiangtang Block, as well as the Xiali Fm. and Late Buqu Fm. in the Yanshiping area of the Qiangtang Block. The decomposition stress on the South Lhasa Block may reflect the northward drift of the Lhasa Block, and its direction of compressive stress in SW may be related to the compression generated by the southward subduction of the Shiquan River-Namtso ocean at this time⁵⁷. The northward compressive stress experienced in the Yanshiping area reflects the northward subduction of the Bangong-Nujiang Ocean, while the southward decomposed stress may reflect the southward flow process of the mantle (Fig. 12). The northward compressive stress experienced in the Yanshiping area is related to the northward subduction of the Bangong-Nujiang Ocean and the northward compression generated by the Central Uplift. However, the Shuanghu area of the Qiangtang Block exhibits the opposite direction by stress, and the southward compressive stress confirms that it is caused by the Central Uplift. The opposite direction of mantle flow in the Qiangtang Block may explain the intra-continent collision caused by bidirectional convection, leading to the re-uplift of the Central Uplift.

Late jurassic

The research strata on the Late Jurassic include the Duodigou Fm. and the Linbuzong Fm. of the Lhasa Block, as well as the Suowa Fm. of the Qiangtang Block. The northward compressive stress of the Duodigou Fm. and Linbuzong Fm. in the Lhasa Block reflects the northward subduction of the Yarlung-Zangbo Neo-Tethys Ocean, while the southward decomposed stress may reflect southward flow of the mantle (Fig. 13). Due to the fact that

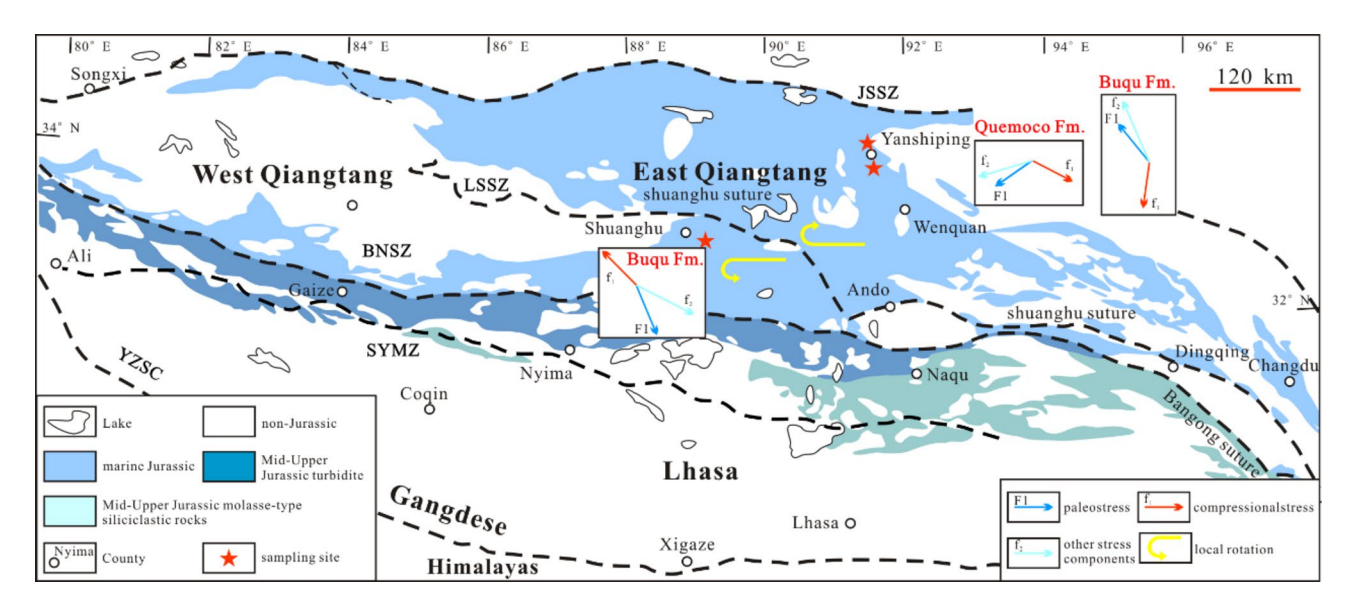


Fig. 11. The stress analysis during the Early Middle Jurassic (Quemoco Fm. and Buqu Fm.).

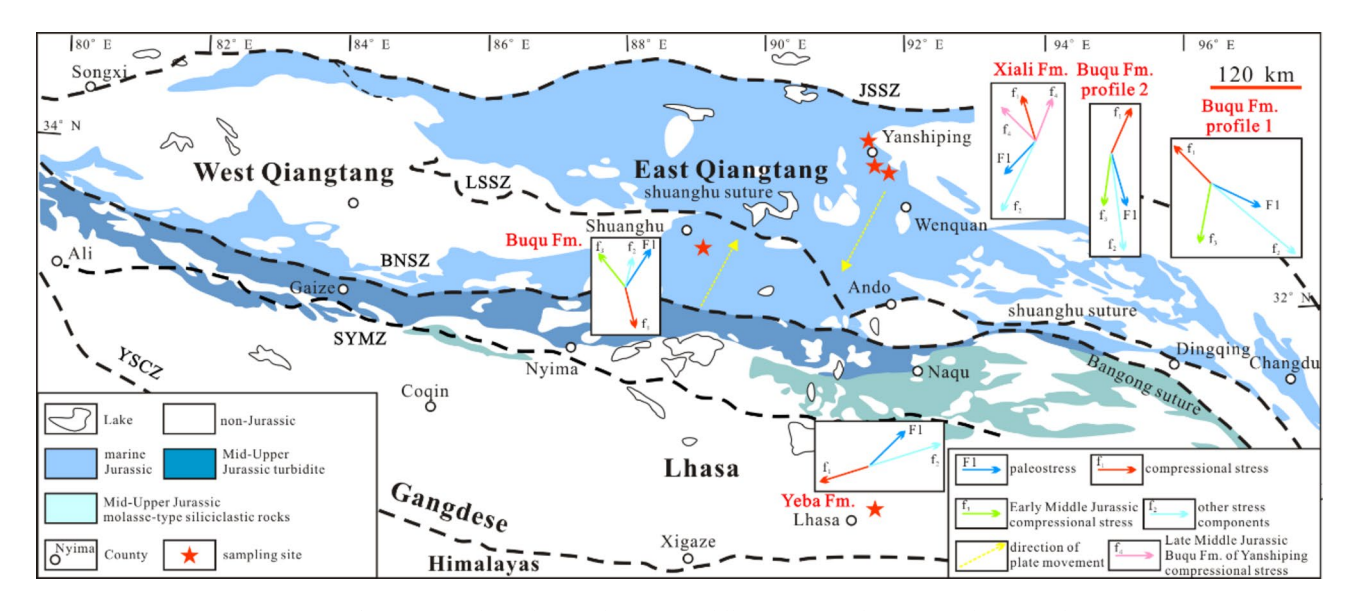


Fig. 12. The stress analysis during the Late Middle Jurassic (Yeba Fm., Xiali Fm. and Buqu Fm.).

the Lhasa Block has not yet collided with the Qiangtang Block at this time, it may be a southward movement with short distance during the northward drift of the Lhasa Block. The southward compressive stress and northward decomposed stress experienced by the Shuanghu area of the Qiangtang Block are the same situation as the late stage of the Middle Jurassic Buqu Fm., indicating a continuation of the tectonic activity of the Qiangtang Block in the Middle Jurassic. At the same time, the direction of early compression and the direction of decomposition stress from the Suowa Fm. in the Yanshiping area are opposite to those in the Shuanghu area, but as the same situation as the Yanshiping area in the late stage of Middle Jurassic. Therefore, it also indicates the continuation including the uplift by the Central Uplift and the northward subduction of the Bangong-Nujiang Tethys Ocean. The movement of Suowa Fm. from the Late Jurassic in the Yanshiping area is opposite, and the southward compressive stress may once again come from the southward compression of the Songpan-Ganzi Terrane under the intra-continent extension of the Qiangtang Block.

Early cretaceous

The research strata on the Early Cretaceous include the Takena Fm. in the Lhasa Block and the Shamulo Fm. in the Bangong-Nujiang suture zone. The southward compressive stress experienced by the Shamulo Fm. reflects the southward subduction of the Bangong-Nujiang Ocean, while the southward compressive stress of the Takena Fm. may also come from the southward subduction of the Bangong-Nujiang Ocean or be related to the southward subduction of the Shiquan River-Namtso small ocean (Fig. 14). There are four views on the structural

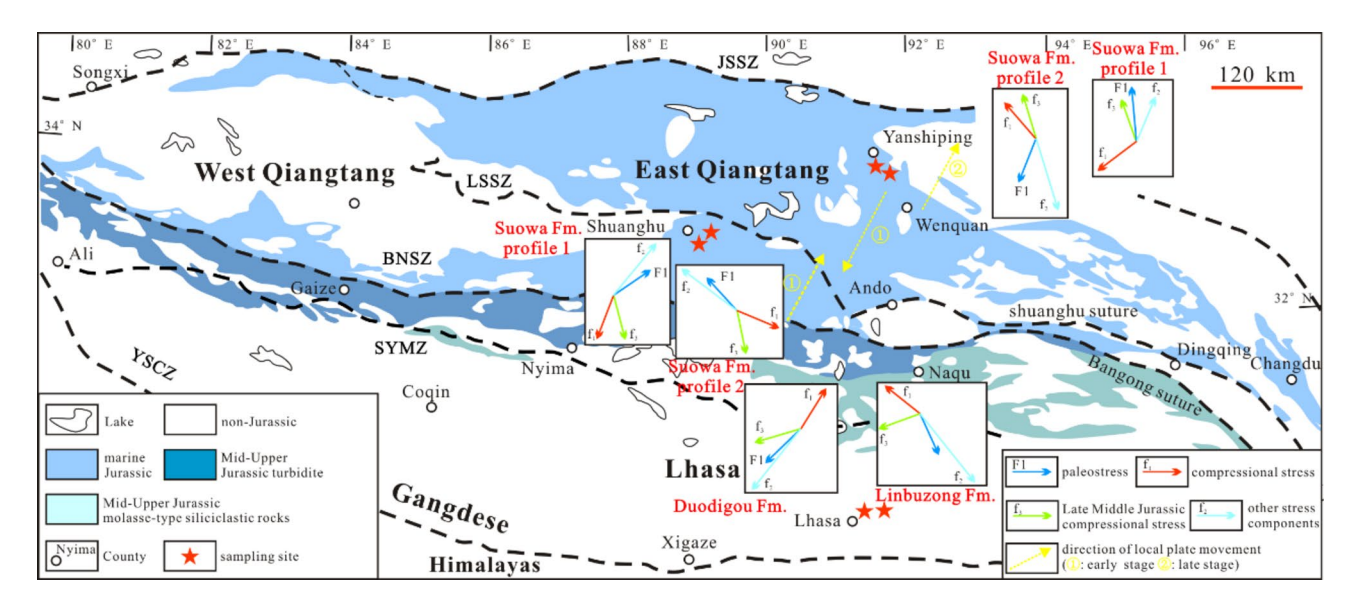


Fig. 13. The stress analysis during the Late Jurassic (Duodigou Fm., Linbuzong Fm. and Suowa Fm.). (Early stage, the decomposition stress reflects mantle convection, leading to the uplift of the Central Uplift. Late stage, the decomposition stress of the South and North Qiangtang blocks is uniformly oriented towards the north, reflecting the northward compression of the Songpan-Ganzi Terrane by the Qiangtang Block.)

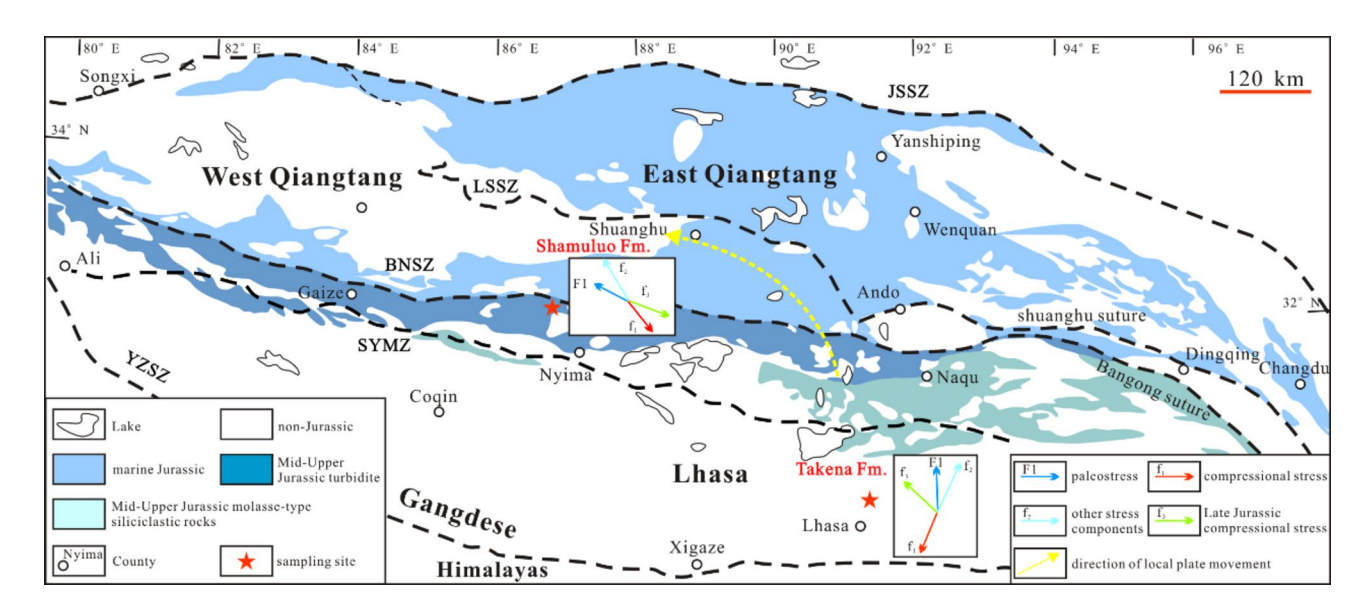


Fig. 14. The stress analysis during the Early Cretaceous (Takena Fm. and Shamuluo Fm.). (Additional stress components have significantly contributed to plate motion dynamics, potentially generated by magmatic flow processes within the lithosphere.)

properties of the Shiquan River-Namtso small ocean: (1) It represents an independent arc-land collision zone⁵⁸; (2) It is an internal branch of the Bangong-Nujiang Tethyan Ocean with the same structural properties⁵⁹; (3) It is the initial expansion basin of the Bangong-Nujiang Tethyan Ocean⁶⁰; (4) It is a thrust-nappe structure that upthrusts southward in the Bangong-Nujiang Tethyan Ocean⁶¹. According to geochemical studies of the ophiolite belt, it is believed that the Bangong-Nujiang Ocean and the Shiquan River-Namtso small ocean have completely different tectonic backgrounds, indicating that the Shiquan River-Namtso ocean is independent of the Bangong-Nujiang Tethyan Ocean⁵⁷.

The argument about the closure time of the Shiquan River-Namtso ocean focuses on the period of Early Cretaceous and Late Cretaceous. The study of Late Cretaceous volcanic rocks in the Shiquan River-Namtso suture zone, including intrusive rocks from the Dongco area (104 Ma) and adakite granite from the Ritu area (101-84Ma)⁶², suggests that these rocks were formed in a collisional tectonic environment. From the perspective of regional stratigraphic unconformity between the Early Cretaceous and Jurassic in the North Lhasa Block, it is also believed that the closure of the Shiquan River-Namtso ocean in the Early Cretaceous led to a transition in

the tectonic background⁵⁷. Therefore, it is believed that the Shiquan River-Namtso ocean was already closed in the Early Cretaceous. However, research on the volcanic rocks of Early Cretaceous Zenong Group and Yongzhu ophiolite (133-114 Ma) in West Namtso suggests that they were not yet closed in the Early Cretaceous. Moreover, Chen et al., (2022)³⁸ when studying the formation and evolution process of the Nyima Basin, believed that the formation of the Nyima Basin was related to the southward subduction of the Bangong-Nujiang Tethyan Ocean that began in the Early Cretaceous and the northward subduction of the Shiquan River-Namtso ocean that began in the Early Cretaceous, indicating that the Shiquan River-Namtso ocean had not yet closed in the Early Cretaceous.

Due to the transition of the subduction polarity from south to north in the Shiquan River-Namtso ocean during the Early Cretaceous, and the intensity of the southward subduction decreased. In addition, the magnetic fabric including strong cleavage and tensile lineation exhibited by the southward compressive stress on the Takena Fm. should be more closely related to the southward subduction of the Bangong-Nujiang Tethyan Ocean. Therefore, it is believed that the southward compression experienced by the Takena Fm. may be related to the southward subduction of the Shiquan River-Namtso ocean, but the main force is still the southward subduction of the Bangong-Nujiang Tethyan Ocean.

Late cretaceous

The research strata on the Late Cretaceous include the Shexing Fm. in the Lhasa Block and the Jingzhushan Fm. on the south side of the Bangong-Nujiang suture zone. According to the analysis of stress direction, the Shexing Fm. is divided into early stage and late stage. The late stage of the Shexing Fm. is in the same period as the Jingzhushan Fm. Due to the intra oceanic arc of the Shiquan River- Namtso ocean being adhered to the northern Gangdise Block by arc-land collision in the Late Jurassic-Early Cretaceous⁶³, and it had already closed and disappeared in the early stage of Late Cretaceous (-113Ma)⁶⁴. Therefore, the southward compressive stress experienced by the Shexing Fm. in the early stage is related to the southward subduction of the Bangong-Nujiang Tethyan Ocean. And the northward compressive stress experienced by the late stage of Shexing Fm. and Jingzhushan Fm. is related to the northward subduction of the Yarlung-Zangbo Neo-Tethys Ocean. In addition, there is a certain change in the direction of decomposition stress experienced by the Lhasa Block. Starting from early stage of the Shexing Fm., the mantle flowed clockwise, with the Jingzhushan Fm. flowing in direction of EN on the northern Lhasa Block and the late stage of the Shexing Fm. flowing in direction of ES on the southern Lhasa Block. Therefore, the drag of the mantle on the Lhasa Block caused it to rotate clockwise (Fig. 15).

Combining paleomagnetism of the Lhasa Block and Qiangtang Block in the Late Cretaceous, the Lhasa Block: $Ds = 350.2^{\circ 65}$, $Ds = 0.9^{\circ 66}$, $Ds = 350.8^{\circ 67}$, $Ds = 312.6^{\circ 12}$, $Ds = 8.2^{\circ 44}$, and the Qiangtang Block: $Ds = 51.3^{\circ 68}$, $Ds = 312.6^{\circ 69}$, $Ds = 68.0^{\circ 70}$, indicating that the above magnetic declinations are all within the clockwise movement. This indicates that the Bangong-Nujiang Tethyan Ocean has closed, as well as the Lhasa and Qiangtang Blocks have also collided into a whole, thus undergoing a unified clockwise rotation.

Closed evolution process of Bangong-Nujiang Tethyan ocean Closure process

(1) northward subduction The compressive stress experienced in the Yanshiping area of the Qiangtang Block during the Middle-Late Jurassic was related to the northward subduction of the Bangong-Nujiang Ocean and the collision between the blocks (Fig. 16). Yanshiping area was subjected to southward compressive stress from the Middle Jurassic Quemoco Fm. to the early stage of Buqu Fm., belonging to two tectonic activities, but both reflected the collision between the Qiangtang Block and the Songpan-Ganzi Terrane. From the Late Buqu Fm.

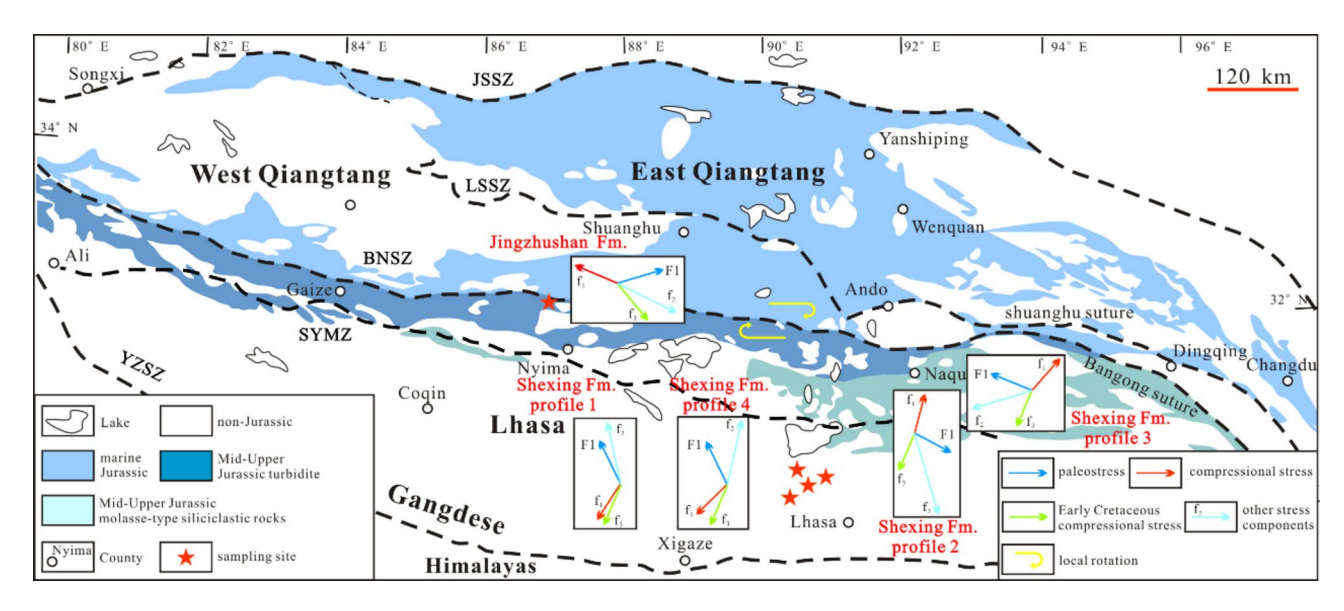


Fig. 15. The stress analysis during the Late Cretaceous (Shexing Fm. and Jingzhushan Fm.).

to the Early Suowa Fm., the North Qiangtang Block was subjected to northward compressive stress, which was related to the northward subduction of the Bangong-Nujiang Ocean. During the Late Suowa Fm., the Qiangtang Block was subjected to southward compressive stress again. Magnetic fabric analysis (Fig. 7m) reveals distinct deformation patterns: the Xiali Fm. (J_2x) exhibits a combination of initial deformation fabric, pencil-like fabric, and strong cleavage fabric. In comparison, the Early Suowa Fm. (J_3s) is primarily characterized by initial deformation fabric and pencil-like fabric (Fig. 7(s) (p)). This contrast in magnetic fabric development indicates a significant reduction in tectonic stress intensity during the deposition of the Early Suowa Fm., suggesting the gradual weakening or termination of the northward subduction of the Bangong-Nujiang Tethyan Ocean. And compared to this, the collision between the Qiangtang Block and the Songpan-Ganzi Terrane is more intense.

(2) transition of the subduction Polarity The Shamulo Fm. is distributed along the Bangong-Nujiang suture zone, and is generally characterized by clastic rocks mixed with limestone, with significant regional phase transi-

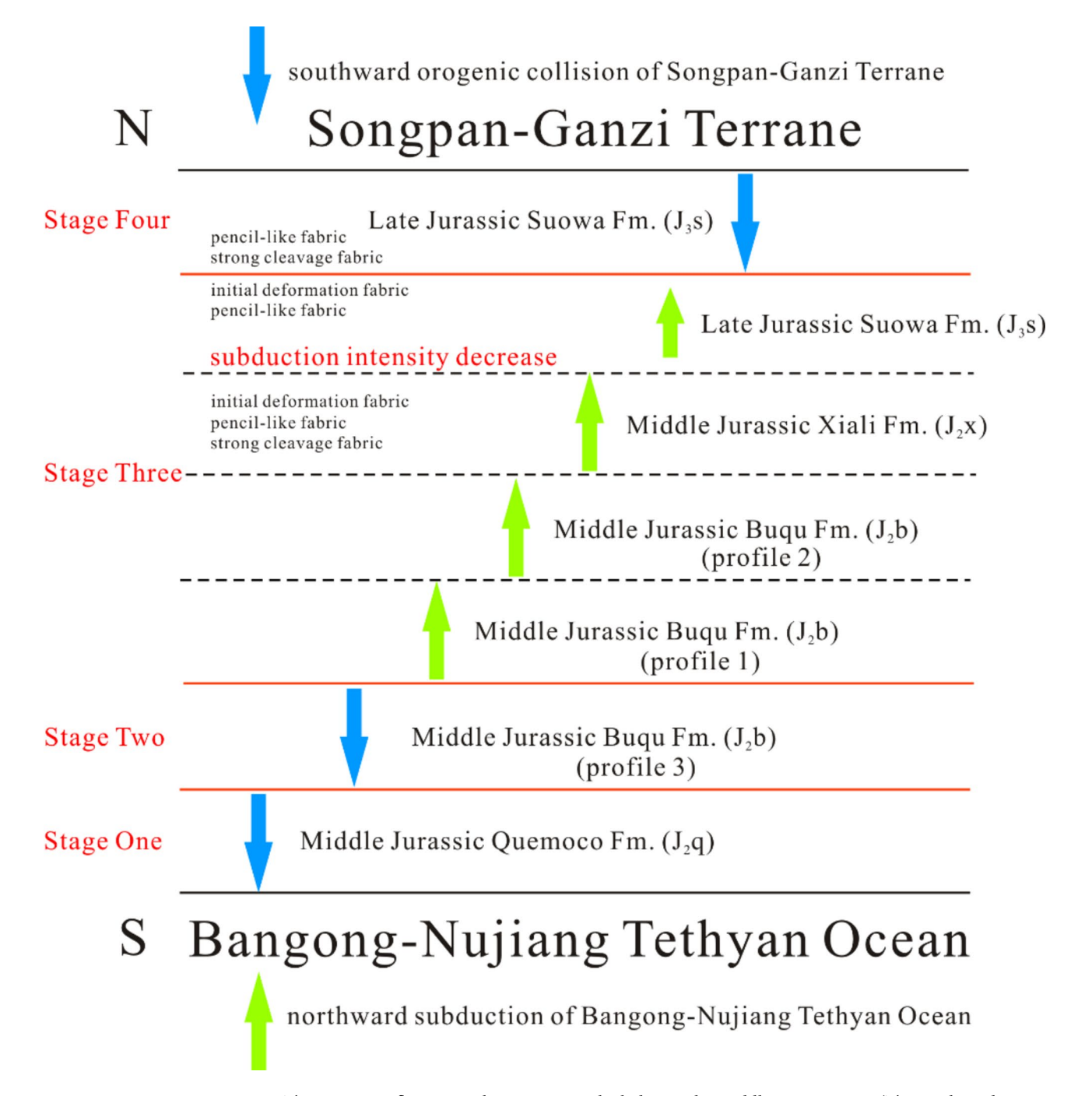


Fig. 16. The tectonic influence on the Qiangtang Block during the Middle-Late Jurassic. (The southward compression is caused by the collision of the Songpan-Ganzi Terrane. The northward compression is caused by the northward subduction of the Bangong-Nujiang Tethyan Ocean.)

tions. Its lithology is divided into two parts, with the lower part consisting of volcanic conglomerate interbedded with fine-grained sandstone and thin layers of calcareous siltstone. Its lithological characteristics are consistent with those of the Shamulo Fm. samples collected in the North Nyima County of this study, while the upper part consists of bioclastic limestone. Petrographic studies have shown that the lower part was formed in a deep-water environment of slope facies, while the upper part was formed in a shallow water environment of estuary-coast⁷¹. After studying the Shamulo Fm. exposed in Geji, Liu et al. (2019)⁷¹ believed that the age distribution of detrital zircons in the lower part is among 200-130 Ma, while the age distribution of detrital zircons in the upper part is among 122-101 Ma. And according to studies of provenance, there are significant differences between the upper and lower parts of the Shamulo Fm. The lower part has similar properties to the South Qiangtang Block, while the upper part has good similarities with both the Lhasa Block and the Qiangtang Block. Compared to the sedimentary study of volcanic breccia at 102.9 Ma and siltstone at 95 Ma in the upper part of the Shamulo Fm., it is believed that the subduction process of the Bangong-Nujiang Ocean conforms to the principles of "closure diachroneity" and "scissor collision". Based on the analysis of stress and tectonic environment for the Middle-Late Jurassic Buqu Fm. and Suowa Fm. in the back-arc basin of South Qiangtang Block, it is believed that the Shamulo Fm. in the Bangong-Nujiang suture zone developed weak island-arc structure during the transition of subduction polarity in the Bangong-Nujiang Tethyan Ocean.

Based on the transition mechanism of subduction polarity⁷² and combined with the research in this study, we believe that the transition process of subduction polarity during the Middle Jurassic-Early Cretaceous in the Bangong-Nujiang Ocean is as follows (Fig. 17): The subduction process of Bangong-Nujiang Ocean mainly includes five critical periods. The first period was the northward subduction of the Bangong-Nujiang oceanic crust beneath the South Qiangtang Block during the deposition of the Buqu Fm. And due to the magmatism including plate melting and mantle upwelling, the Shuanghu area (back-arc basin) developed an extensional environment. The second period was during the deposition of the Late Jurassic Suowa Fm., when the northward subduction of the oceanic crust weakened and gradually ceased. And the collision orogeny between the North and South Qiangtang Blocks has intensified, resulting in a compressional environment in the back-arc basin. The third period was the occurrence of intra-oceanic subduction in the Bangong-Nujiang Ocean, which developed the volcanic arc of the Shamulo Fm. At the same time, volcanic arcs were stretched again due to mantle upwelling, creating an extensional environment. This period was the development time of the lower part of the Shamulo Fm., mainly characterized by deep-water slope facies and the development of carbonate rocks. The fourth period was the development of the upper part of the Shamulo Fm., where the northward subducting plate within the Bangong-Nujiang Ocean experienced detachment and sunk into the mantle. Additionally, the volcanic arc of the Shamulo Fm. collided with the North Lhasa Block, accompanied by the development of estuary-coast shallow water deposition. In the fifth period, during the late stage of upper part in the Shamulo Fm., a new subducting plate was formed in the Bangong-Nujiang oceanic crust, which began to subduct southward. This part is exactly the Shamulo Fm. sampled in the study. Subduction, detachment, and melting of oceanic crust produced magma activities, leading to volcanic breccia eruptions and intermittent deposition of siltstone. At this point, subduction polarity of Bangong-Nujiang Tethyan Ocean has completely changed from north to south. Therefore, the transition time of the subduction polarity in the Bangong-Nujiang Ocean is limited at 102.9-95 Ma.

(3) Southward subduction

The northward compressive stress experienced by the Lhasa Block came from the northward subduction of the Neo-Tethys Ocean, while the southward compressive stress came from the southward subduction of the Bangong-Nujiang Ocean or Shiquan River-Namtso ocean (Fig. 18). Therefore, during the Middle Jurassic Yeba Fm., the Linzhou Basin was subjected to compressive stress in direction of WWS, which gradually weakened. It is considered to be more closely related to the southward subduction of the Shiquan River-Namtso ocean and to be in the late stage of subduction. During the Late Jurassic, the Linzhou Basin was mainly subjected to northward compressive stress, which is considered to be related to the northward subduction of the Neo-Tethys Ocean. Due to the closure of the Shiquan River-Namtso ocean in the Early Cretaceous, it was related to the southward subduction of the Bangong-Nujiang Ocean at this time. At the same time, the southward compressive stress experienced in the early stage of Late Cretaceous also came from the southward subduction of the Bangong-Nujiang Ocean. In the Late Cretaceous, the Linzhou Basin was subjected to northward compressive stress again due to the northward subduction of the Neo-Tethys Ocean, indicating that the Bangong-Nujiang Ocean had already closed.

(4) end of the subduction The Dickinson diagram⁷³ shows that the red-layer samples from the Jingzhushan Fm. in the Nyima Basin mainly developed in the magmatic island-arc environments (Fig. 19), indicating that the tectonic environment is dominated by magmatic island-arc on active continental margins and has undergone long-term erosion, rather than the tectonic background of cyclic orogenic belt. Based on the developed thrust-nappe structures in the basin, it is believed that the mechanism of "arc-arc" soft collision is more suitable for the formation mode of the Nyima Basin, rather than the faulted basin under the background of traditional "land-land" collision (Fig. 19b). The essence of its structure is the soft collision between the volcanic rocks from the Qushenla Fm⁷⁴ generated by the southward subduction of the Bangong-Nujiang Ocean in the late stage of Early Cretaceous under the northward subduction of the Yarlung-Zangbo Neo-Tethys Ocean and the northward drag of the mantle on the Lhasa Block, and the arc-land "overlap zone" of the South Qiangtang Block under southward stretching⁵⁴, and the deposition front area of the Bangong-Nujiang Ocean formed under erosion. At the same time, there are many metamorphic debris fragments in the mineral photos, such as quartz debris or schist debris under recrystallization, which also indicates that the sandstone minerals of the Jingzhushan Fm. came more from arc magma (Fig. 19c).

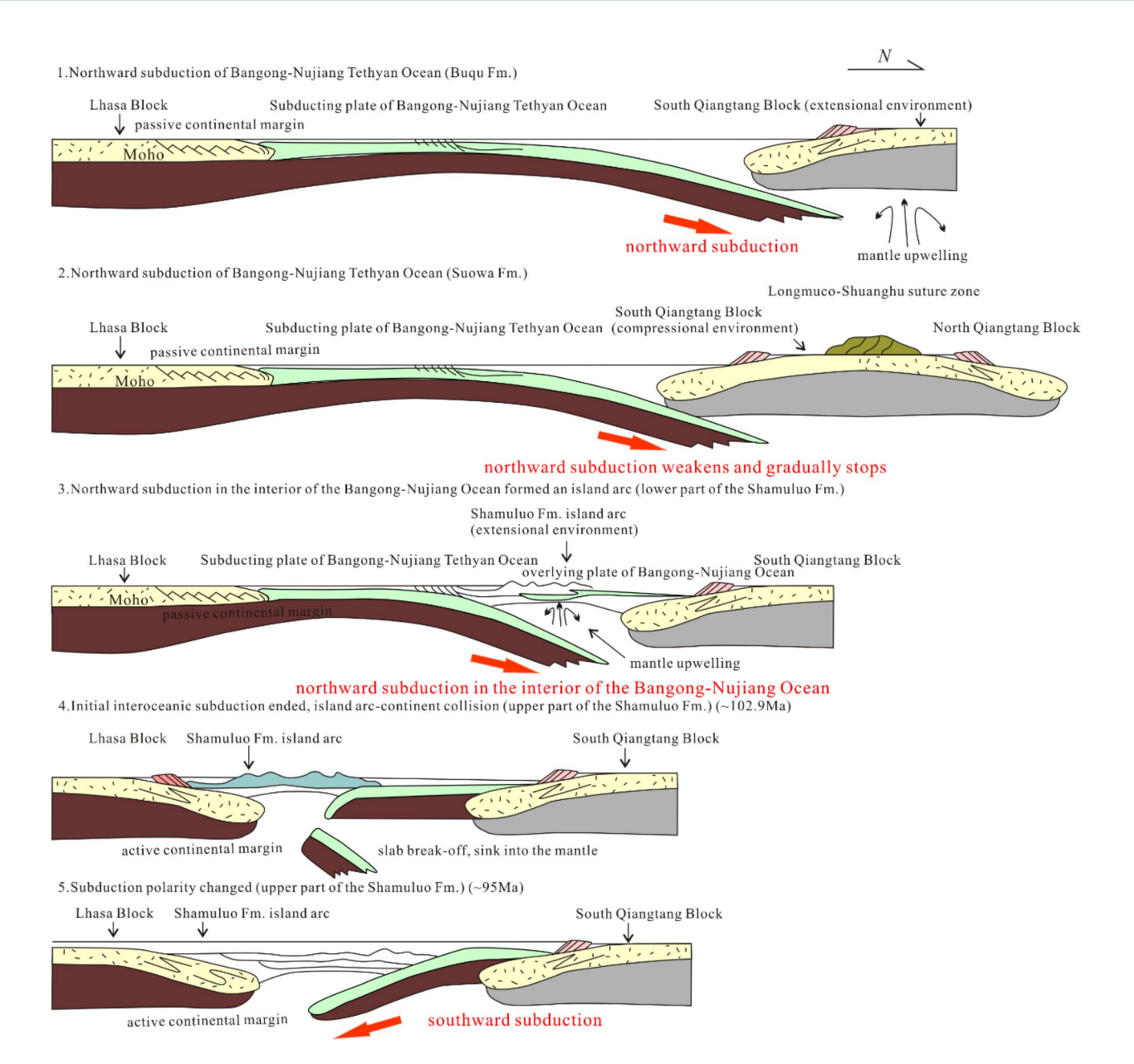


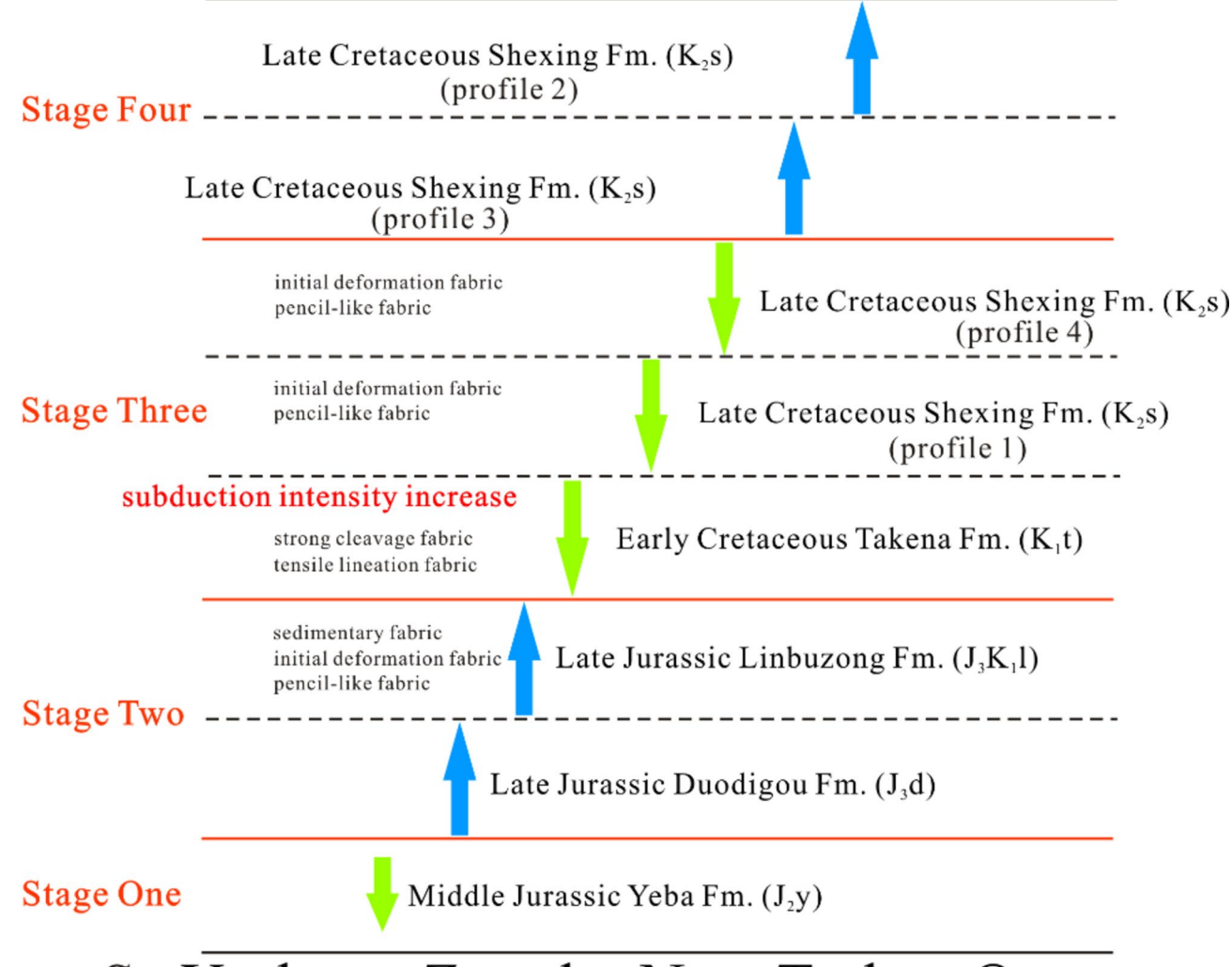
Fig. 17. Transition of subduction process in the Bangong-Nujiang Tethyan Ocean from the Middle Jurassic (Buqu Fm.) to the Early Cretaceous (Shamuluo Fm.).

Closure time

The research on the closure time and closure process of Bangong-Nujiang Ocean mainly focuses on the perspectives of "closure diachroneity" and "scissor collision". The closure times from east to west are 116.6±0.8 Ma, 120±1.4 Ma, 107.8±8.1 Ma, and 96.0±1.1 Ma, respectively ⁷⁵. According to the research in this study, during the deposition period of the Shamulo Fm. in the Bangong-Nujiang suture zone, the Bangong-Nujiang Ocean had completed the transition of subduction polarity and was in the late stage of closure. Meanwhile, analysis of the provenance indicates that the North Lhasa Block and the South Qiangtang Block are both source areas of the Shamulo Fm. The material exchange between the Lhasa Block, Qiangtang Block, and Bangong-Nujiang suture zone marks the disappearance of the deep-sea shelf. Research on the tectonic background shows that the detrital zircons of the Shamulo Fm. reveal that the most samples is in a collision background and a few are in a convergence background, and the convergence background occurred earlier than the collision background (Fig. 20). This method reflects the different tectonic backgrounds of deposition basins in which detrital zircons are located by the difference between the crystallization age of detrital zircons and the age of deposition strata ⁷⁶. The convergence background and collision background reflect the process of southward subduction and extinction of the Bangong-Nujiang Ocean, as well as the collision between the Lhasa Block and the South Qiangtang Block. This also indicates that the Shamulo Fm. (Early Cretaceous) in this study should be the late



N BangongCo-Nujiang Tethyan Ocean



Yarlung-Zangbo Neo-Tethys Ocean



Fig. 18. The tectonic influence on the Lhasa Block from the Middle Jurassic to the Late Cretaceous. (The southward extrusion is caused by the southward subduction of the Bangong-Nujiang Tethyan Ocean. The northward extrusion is caused by the northward subduction of the Yarlung-Zangbo Neo-Tethys Ocean.)

stage of the subduction and disappearance of the Bangong-Nujiang Ocean. Research of magnetic fabric shows that sandstone of the Shamulo Fm. developed initial deformation fabric, indicating a relatively stable deposition environment. Compared with the strong deformation fabrics in the Buqu Fm and Suowa Fm., it indicates a weakening of tectonic activity. The volcanic breccia of the Shamulo Fm. in the Bangong-Nujiang suture zone at 102.9 Ma is related to magmatism during the plate subduction. Moreover, the clastic sandstone of the Shamulo Fm. at 112 Ma was subjected to southward compressive stress, indicating that the Bangong-Nujiang Ocean had already begun southward subduction at 112 Ma, and the transition time of subduction polarity was limited to among 112-102.9 Ma.Geochronological investigations of the Late Cretaceous Shexing Fm. reveal multiple depositional phases, with age clusters at 83-78Ma⁷⁷, 104-72Ma⁷⁸, 110-72Ma⁷⁹, and a distinct 98 Ma horizon at the formation's top80. Furthermore, tectonic analysis indicates that the Linzhou Basin experienced structural

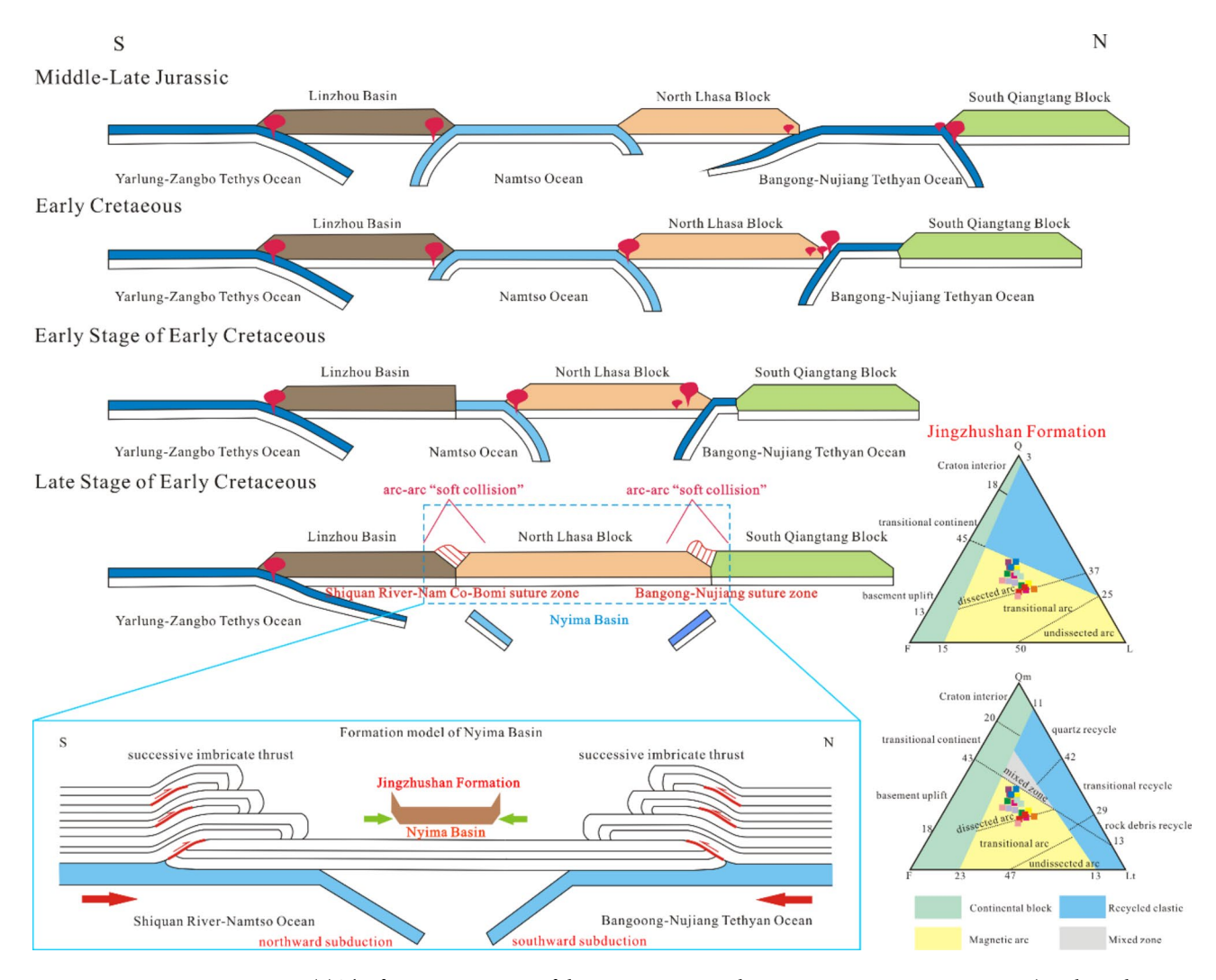


Fig. 19. (a) The formation process of the Nyima Basin in the Bangong-Nujiang suture zone. (Marking the closure of Bangong-Nujiang Tethyan Ocean.) (b) The formation mechanism of thrust-nappe structure in the Nyima Basin. (c) Analysis of the tectonic background based on Q-F-L and Qm-F-Lt diagrams⁷².

inversion at approximately 96 Ma, coinciding with regional compressional events 81 . Integrating these findings with the well-constrained 92 Ma age from the Jingzhushan Fm 38 , we have constrained the subduction and closure of the Bangong-Nujiang Tethyan Ocean to the period between 105 and 92 Ma, with the terminal closure occurring post -112 Ma.

Additionally, paleomagnetic analysis of the Early Late Cretaceous red beds from the Shexing Fm. in the Lhasa Block has revealed a paleomagnetic pole position at 75.0° N, 306.7° E, indicating a paleolatitude of 15° N⁶⁷. The study by Chen et al., (2017) on the Gaize area of the Qiangtang Block reveals a Late Cretaceous pole position at 45.4° N, 348.1° E, corresponding to a paleolatitude of 18.6° N⁶⁵. Meng et al., (2018) obtained a Late Cretaceous pole position at 29.2° N, 171.8° E in the Shuanghu area of the Qiangtang Block, corresponding to a paleolatitude of 20.8° 6. The paleomagnetic evidence from these studies demonstrates that the Lhasa and Qiangtang Blocks had already amalgamated by this period, indicating the complete closure of the Bangong-Nujiang Tethyan Ocean. Chen et al. (2017) conducted geochronological analyses³⁸ on both volcanic rocks and red sandstone samples, yielding distinct age constraints. The volcanic rocks were precisely dated to 103.8 ± 0.46 Ma (Early Cretaceous), while the red sandstone was attributed to the Late Cretaceous⁶⁹. Based on these robust geochronological data, the closure of the Bangong-Nujiang Tethyan Ocean can be confidently constrained to the period between 103.8 and 92 Ma.

Conclusions

This study integrates multi-method constraints from systematic AMS analyses across the Central Tibetan Plateau and zircon U-Pb geochronology of the Shamuluo Fm. within the Bangong-Nujiang suture zone to precisely reconstruct the closure timing and kinematic evolution of the Bangong-Nujiang Tethyan Ocean. The following key findings are established:

(1) The compressive stress orientations revealed by AMS records reflect dynamic interactions between the Lhasa and Qiangtang Blocks during the subduction dynamics of the Bangong-Nujiang Tethyan Ocean.

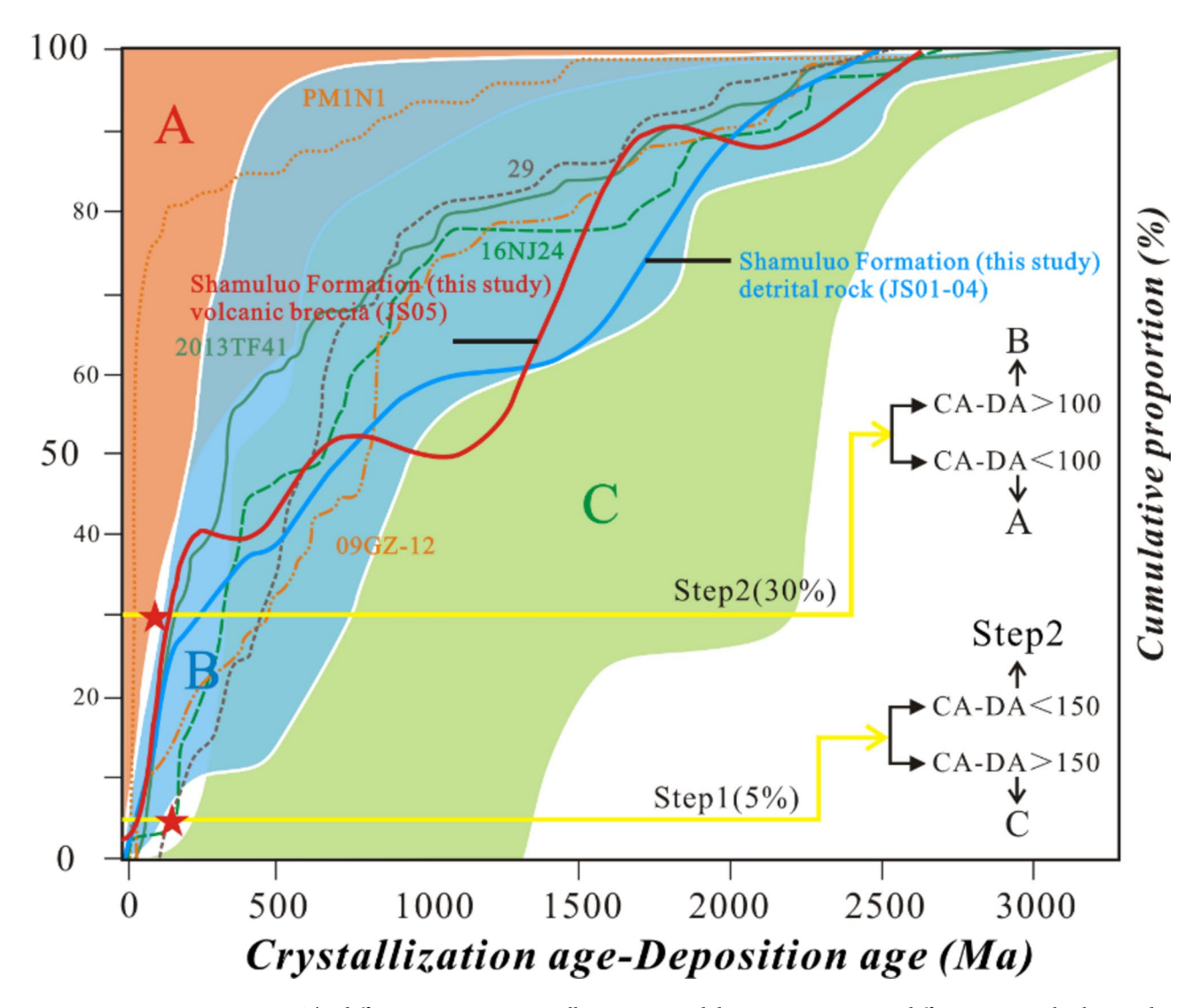


Fig. 20. The differences in zircon crystallization age and deposition age among different tectonic backgrounds in the Shamulo Fm.

Specifically: The Southern Qiangtang Block experienced northward compression during the Middle-Late Jurassic due to the Bangong-Nujiang Tethyan Ocean's northward subduction, whereas the Southern Lhasa Block's southward compressional deformation during the Cretaceous was driven by the opposing subduction of both the Bangong-Nujiang Tethyan Ocean (southward) and the Yarlung-Zangbo Neo-Tethys Ocean (northward).

(2) The Bangong-Nujiang Tethyan Ocean experienced a multi-stage tectonic evolution, beginning with northward subduction during the Middle-Late Jurassic. A significant transition in subduction polarity occurred from the Late Jurassic to Early Cretaceous (112-102.9 Ma), ultimately establishing southward subduction in the Early Cretaceous. This southward subduction continued until the Early Shexing Fm. deposition in the Late Cretaceous (103.8–92 Ma), when it ceased following the closure of the central Bangong-Nujiang Tethyan Ocean. This closure event led to the final amalgamation of the Lhasa and Qiangtang Blocks, marking a crucial stage in the tectonic evolution of the region.

Data availability

The datasets used and/or analysed during the current study available from the corresponding author on reasonable request.

Received: 7 November 2024; Accepted: 23 April 2025

Published online: 14 May 2025

References

1. Zhu, R. X., Zhao, P., Wan, B. & Sun, W. D. Geodynamics of the one-way subduction of the Neo-Tethys ocean (in Chinese). *Chin. Sci. Bull.* **68**, 1699–1708. https://doi.org/10.1360/TB-2022-1141 (2023).

- 2. Huang, S. H. et al. Geochemical characteristics of Early Cretaceous magmatic rocks in the northwestern part of the Lhasa Block and indications of early crustal growth of the southern plateau. Geochimica. 49(1): 21–35. https://doi.10.19700/j.0379-1726.01.002 (2020). (2020).
- 3. Chen, S. M. et al. Crustal evolution constraints from the petrogenesis of late cretaceous Konglong volcanics on Southern margin of central Lhasa subterrane. *Geoscience* 35 (6), 1713–1726. https://doi.org/10.19657/j.geoscience.1000-8527.2021.126 (2021).
- 4. Li, Y., Zhang, S. Z., Li, F. Q., Qin, Y. D. & Geochronology Geochemistry and petrogenesis of late jurassic granitoids in Shiquanhe area, Western Lhasa Blcok. *Tibet Earth Sci.* **45** (8). https://doi.org/10.3799/dqkx.2020.102 (2020).
- 5. Li, S. M. et al. One or two Early Cretaceous arc system in the Lhasa Terrane, Southern Tibet. Journal of Geophysical Research: Solid Earth. 123. https://doi.10.1002/JB015582 (2018). (2018).
- Zhang, L. L. et al. Sr-Nd-Hf isotopes of the intrusive rocks in the cretaceous Xigaze ophiolite, Southern Tibet: constraints on its formation setting. Lithos 258–259, 133–148. https://doi.org/10.1016/j.lithos.2016.04.026 (2016).
- 7. Zhai, Q. G. et al. SHRIMP Zircon U-Pb geochronology, geochemistry and Sr-Nd-Hf isotopic compositions of a mafic Dyke swarm in the Qiangtang Terrane, Northern Tibet and geodynamics implications. *Lithos* 174, 28–43. https://doi.org/10.1016/j.lithos.2012. 10.018 (2013).
- 8. Chen et al. Combined paleomagnetic and geochronological study on cretaceous strata of the Qiangtang Terrane, central Tibet. *Gondwana Res.* 41, 373–389. https://doi.org/10.1016/j.gr.2015.07.004 (2017).
- 9. Sun, Z. M. et al. New early cretaceous paleomagnetic data from volcanic of the Eastern Lhasa block and its tectonic implications. *Acta Petrologica Sinica*. 24 (7), 1621–1626 (2008).
- Chen, W. et al. Paleomagnetic results from the early cretaceous Zenong group volcanic rocks, Cuoqin, Tibet, and their paleogeographic implications. Gondwana Res. 22, 461–469. https://doi.org/10.1016/j.gr.2011.07.019 (2012).
- 11. Ma, Y. M. et al. Paleomagnetism and U-Pb Zircon geochronology of lower cretaceous lava flows from the Western Lhasa Terrane: new constraints on the India-Asia collision process and intracontinental deformation within Asia. *J. Geophys. Research: Solid Earth.* 119, 7404–7424. https://doi.org/10.1002.2014JB011362 (2014).
- 12. Yang, T. S. et al. New insights into the India-Asia collision process from cretaceous paleomagnetic and geochronology results in the Lhasa terrane. *Gondwana Res.* 28 (2), 625–641. https://doi.org/10.1016/j.gr.2014.06.010 (2015).
- 13. Bian, W. et al. New early cretaceous paleomagnetic and geochronological results from the Far Western Lhasa Terrane: contributions to the Lhasa-Qiangtang collision. *Sci. Rep.* 7, 16216. https://doi.org/10.1038/s41598-017-16482-3 (2017).
- 14. Li, Z. Y. et al. Paleomagnetic constraints on the paleolatitude of the Lhasa block during the early cretaceous: implications for the onset of the India-Asia collision and latitudinal shortening estimates across Tibet and stable Asia. *Gondwana Res.* 41, 352–372. https://doi.org/10.1016/j.gr.2015.05.013 (2017).
- 15. Ma, A. L. et al. Sedimentary and tectonic evolution of the Southern Qiangtang basin: implications for the Lhasa-Qiangtang collision timing. *J. Geophys. Research: Solid Earth.* 122 (7), 4790–4813. https://doi.org/10.1002/2017JB014211 (2017).
- Kapp, P. et al. Geological records of the Lhasa-Qiangtang and Indo-Asian collisions in the Nima area of central Tibet. Geol. Soc. Am. Bull. 119 (7-8), 917-933. https://doi.org/10.1130/B26033.1 (2007).
- 17. Wang, K. et al. Magnetic fabric and structural deformation. Chin. J. Geophys. (in Chinese). 60 (3), 1007–1026. https://doi.org/10.6 038/cig20170315 (2017).
- 18. Mattei, M. et al. Magnetic fabric of weakly deformed clay-rich sediments in the Italian Peninsula: relationship with compressional and extensional tectonics. 271(1-2): 107-122. (1997). https://doi.org/10.1016/S0040-1951(96)00244-2
- Cifelli, F. et al. The origin of tectonic lineation in extensional basins: combined neutron texture and magnetic analyses on undeformed clays. Earth Planet. Sci. Lett. 235 (1–2), 62–78. https://doi.org/10.1016/j.epsl.2005.02.042 (2005).
- Borradaile, G. J. & Hamilton, T. Magnetic fabric May proxy as neotectonic stress trajectories, polis rift. Cyprus Tectonics. 23 (1), TC1001. https://doi.org/10.1029/2002TC001434 (2004).
- 21. Scheepers, P. J. J. et al. Magnetic fabric of pleistocene clays from the tyrrhenian Arc: A magnetic lineation induced in the final stage of the middle pleistocene compressive event. *Tectonics* 13 (5), 1190–1200. https://doi.org/10.1029/94TC00221 (1994).
- 22. Tarling, D. & Hrouda, F. Magnetic Anisotropy of Rocks (Springer Science & Business Media, 1993).
- 23. Saint-Bezar, B. et al. Magnetic fabric and petrographic investigation of hematite-bearing sandstones within ramp-related folds: examples from the South atlas front (Morocco). *J. Struct. Geol.* **24** (9), 1507–1520. https://doi.org/10.1016/S0191-8141(01)00140-7 (2002).
- 24. Li, S. H. et al. Anisotropy of magnetic susceptibility (AMS) analysis of the Gonjo basin as an independent constraint to date Tibetan shortening pulses. *Geophys. Res. Lett.* 47 (8). https://doi.org/10.1029/2020GL087531 (2020).
- 25. Fu, Q. et al. Inverse magnetic fabric of remagnetized limestones in the Zaduo area, Eastern Qiangtang Terrane: implications for oroclinal bending in the Eastern Himalayan syntaxis. *Tectonophysics* 871. https://doi.org/10.1016/j.tecto.2023.230175 (2024).
- Luo, L., Qi, J. F. & Zhang, M. Z. AMS investigation in the Pingluoba and Qiongxi anticlines, Sichuan, China: implications for deformation mechanism of the Qiongxi structure. *Tectonophysics* 626, 186–196. https://doi.org/10.1016/j.tecto.2014.04.031 (2014).
- 27. Cao, X. W. et al. The investigations of the deformation of the great counter thrust (GCT) in Zedang area, South Tibet: A case study of magnetic fabric and EBSD analysis. *Acta Petrologica Sinica*. 37 (10), 3167–3184. https://doi.org/10.18654/1000-0569/2021.10.12
- 28. Zhu, D. C. et al. The origin and pre-Cenozoic evolution of the Tibetan plateau. Gondwana Res. 23 (4), 1429–1454. https://doi.org/10.1016/j.gr.2012.02.002 (2013).
- Cao, Y. et al. Paleomagnetism and U-Pb geochronology of early cretaceous volcanic rocks from the Qiangtang block, Tibetan plateau: implications for the Qiangtang-Lhasa collision. *Tectonophysics* 789. https://doi.org/10.1016/j.tecto.2020.228500 (2020).
- 30. Zhu, R. X., Zhao, P. & Zhao, L. Tectonic evolution and geodynamics of the Neo-Tethys ocean. Sci. China Earth Sci. 65 (1), 1–24. https://doi.org/10.1007/s11430-021-9845-7 (2022).
- 31. Zhu, D. C. et al. Raising the Gangdese mountains in Southern Tibet. J. Geophys. Research: Solid Earth. 122 (1), 214–223. https://doi.org/10.1002/2016JB013508 (2017).
- 32. Li, C., Zhai, Q. G., Dong, Y. S. & Huang, X. P. Discovery of eclogite and its geological significance in Qiangtang area, central Tibet. 51: 1095–1100. Chinese Science Bulletin. (2006). https://doi.org/10.1007/s11434-006-1095-3
- 33. Song, P. P. et al. Late triassic paleolatitude of the Qiangtang block: implications for the closure of the Paleo-Tethys ocean. *Earth Planet. Sci. Lett.* **424** (15), 69–83. https://doi.org/10.1016/j.epsl.2015.05.020 (2015).
- 34. Chen, Y. L. et al. U-Pb dating, geochemistry, and tectonic implications of the Songpan-Ganzi block and the longmen Shan, China. *Geochem. J.* 43 (2), 77–99. https://doi.org/10.2343/geochemj.1.009 (2009).
- Shi, Z. X. et al. Bidirectional subduction of the Bangong-Nujiang ocean revealed by deep-crustal seismic reflection profile. Tectonophysics 837 (20). https://doi.org/10.1016/j.tecto.2022.229455 (2022).
- 36. Ma, A. L. et al. The disappearance of a late jurassic remnant sea in the Southern Qiangtang block (Shamuluo formation, Najiangco area): implications for the tectonic uplift of central Tibet. *Palaeogeogr., Palaeoclimatol. Palaeoecol.* **506** (1), 30–47. https://doi.org/10.1016/j.palaeo.2018.06.005 (2018).
- Li, C. et al. High-pressure eclogite-blueschist metamorphic belt and closure of paleo-Tethys ocean in central Qiangtang, Qinghai-Tibet plateau. J. Earth Sci. 20, 209–218. https://doi.org/10.1007/s12583-009-0021-4 (2009).
- 38. Chen, Q. L. et al. Thrust structure and bidirectional paleocurrent in the Jingzhushan formation during the late cretaceous in the Nyima basin, Tibet plateau, China: approach of magnetic fabric and Zircon chronology. *Minerals* 12 (10), 1225. https://doi.org/10.3390/min12101225 (2022).

- 39. Sun, W. D. The magma Engine and the driving force of plate tectonics (in Chinese). Chin Sci Bull, 64, 2988–3006, https://doi.10.1 360/N972019-00274 (2019).
- 40. Yin, A. & Harrison, T. M. Geological evolutions of the Himalayan-Tibetan orogen. *Annu. Rev. Earth Planet. Sci.* 28 (1), 211–280. https://doi.org/10.1146/annurev.earth.28.1.211 (2000).
- 41. Han, K. et al. Geochemistry, chronology and Zircon Lu-Hf isotopic characteristics of the volcanic rocks of Yeba formation in riduo area on the Southern margin of Lhasa Massif and their geological significance. *Geol. Bull. China.* 37 (8), 1554–1570 (2018).
- 42. Song, Y. H. et al. Petrogenesis of volcanic rocks from the Yeba formation in Jialulang area, Tibet and its constraints on the subduction of Neo-Tethyan oceanic slab. *Earth Sci.* 44 (7), 2319–2338. https://doi.org/10.3799/dqkx.2019.147 (2019).
- 43. Zhou, Y. et al. Detrital Zircon U-Pb chronology and geological significance of the middle jurassic Quesangwenquan formation in Linzhou basin, Tibet. Sediment. Geol. Tethyan Geol. https://doi.org/10.19826/j.cnki.1009-3850.2021.06001 (2021).
- 44. BouDagher-Fadel, M. K. et al. Foraminiferal biostratigraphy and palaeoenvironmental analysis of the Mid-Cretaceous limestones in the Southern Tibetan plateau. *J. Foraminifer. Res.* 47 (2), 188–207. https://doi.org/10.2113/gsjfr.47.2.188 (2017).
- 45. Cao, Y. et al. New late cretaceous paleomagnetic data from volcanic rocks and red beds from the Lhasa terrane and its implications for the paleolatitude of the Southern margin of Asia prior to the collision with India. *Gondwana Res.* 41, 337–351. https://doi.org/10.1016/j.gr.2015.11.006 (2017).
- 46. Cheng, L. L. et al. Astrochronology of the middle jurassic Buqu formation (Tibet, China) and its implications for the Bathonian time scale. *Palaeogeogr.*, *Palaeoclimatol. Palaeoecol.* **487**, 51–58. https://doi.org/10.1016/j.palaeo.2017.08.018 (2017).
- 47. Li, X. R. et al. New insights into the late triassic Nadigangri formation of Northern Qiangtang, Tibet, China: constraints from U-Pb ages and hf isotopes Od detrital and magmatic zircons. *Acta Geol. Sinica.* 92 (4), 1451–1467. https://doi.org/10.1111/1755-6724.1 3637 (2018)
- 48. Song, C. H. et al. Sedimentary conditions of evaporites in the late jurassic Xiali formation, Qiangtang basin: evidence from geochemistry records. *Acta Geol. Sinica.* **91** (1), 156–174. https://doi.org/10.1111/1756-6724.13069 (2017).
- 49. Yin, J. R. Bathonian-Callovian (Middle Jurassic) ammonites from Northwestern Qiangtang block, Tibet, and the revised age of the Suowa formation. *Proc. Geologists' Association*. **127** (2), 247–265. https://doi.org/10.1016/j.pgeola.2016.02.005 (2016).
- Yang, R. F. et al. Marine to brackish depositional environments of the Jurassic-Cretaceous Suowa Formation, Qiangtang Basin (Tibet), China. Palaeoclimatology Palaeoecology 473(1): 41–56. https://doi.org/10.1016/j.palaeo.2017.02.031 (2017).
- 51. Luo, A. B. et al. From arc-continent collision to ocean closure: lower cretaceous Shamuluo formation in the Western segment of the Bangong-Nujiang suture zone, central Tibet. *Geosci. Front.* 12 (5). https://doi.org/10.1016/j.gsf.2021.101207 (2021).
- 52. Ma, A. L. et al. The disappearance of a late jurassic remnant sea in the Southern Qiangtang block (Shamuluo formation, Najiangco area): implications for the tectonic uplift of central Tibet. *Palaeogeogr., Palaeoclimatol. Palaeoecol.* **506**, 30–47. https://doi.org/10.1016/j.palaeo.2018.06.005 (2018).
- 53. Li, S. et al. The subduction-accretion history of the Bangong-Nujang Ocean: constraints from provenance and geochronology of the mesozoic strata near Gaize, central Tibet. *Tectonophysics* 702, 42–60. https://doi.org/10.1016/j.tecto.2017.02.023 (2017).
- 54. Li, S. et al. Provenance of mesozoic clastic rocks within the Bangong-Nujiang suture zone, central Tibet: implications for the age of the initial Lhasa-Qiangtang collision. J. Asian Earth Sci. 147, 469–484. https://doi.org/10.1016/j.jseaes.2017.08.019 (2017).
- 55. Bian, W. W. et al. Paleomagnetism of the late cretaceous red beds from the Far Western Lhasa Terrane: inclination discrepancy and tectonic implications. *Tectonics* 39 (8). https://doi.org/10.1029/2020TC006280 (2020).
- 56. Fang, X. M. et al. Mesozoic litho-and magneto-stratigraphic evidence from the central Tibetan plateau for Megamonsoon evolution and potential evaporites. *Gondwana Res.* 37, 110–129. https://doi.org/10.1016/j.gr.2016.05.012 (2016).
- 57. Gao, K. et al. Geochronology, petrogeochemistry, and tectonic setting of cretaceous granitoids in the Zanzongcuo zone, Northern Tibet, China. *Geochem. Int.* 57, 424–437. https://doi.org/10.1134/S0016702919040062 (2019).
- 58. Wang, B. D. et al. Spatial-temporal framework of Shiquanhe-Laguoco-Yongzhu-Jiali ophiolite melange zone, Qinghai-Tibet plateau and its tectonic evolution. *Earth Sci.* 45 (8), 2764–2784. https://doi.org/10.3799/dqkx.2020.083 (2020).
- 59. Pan, G. T. et al. Tectonic evolution of the Qinghai-Tibet plateau. J. Asian Earth Sci. 53, 3–14. https://doi.org/10.1016/j.jseaes.2011. 12.018 (2012).
- 60. Zhang, S. Q., Qi, X. X., Wei, C., Chen, S. Y. & Geochemistry Zircon U-Pb dating and hf isotope compositions of early cretaceous magmatic rocks in Yongzhu area, Northern Lhasa Terrane, Tibet, and its geological significance. *Earth Sci.* 43 (4), 1085–1109. https://doi.org/10.3700/dqkx.2018.711 (2018).
- 61. Zeng, Y. C. et al. Geochronological and geochemical constraints on the origin of the Yunzhug ophiolite in the Shiquanhe-Yunzhug-Namu Tso ophiolite belt, Lhasa Terrane, Tibetan plateau. *Lithos* 300–301, 250–260. https://doi.org/10.1016/j.lithos.2017.11.025 (2018).
- 62. Kapp, P. et al. Mesozoic and cenozoic tectonic evolution of the Shiquanhe area of Western Tibet. *Tectonics* 22 (4), 1029. https://doi.org/10.1029/2001TC001332 (2003).
- 63. Liu, W. L. et al. Age and composition of the Rebang Co and Julu ophiolites, central Tibet: implications for the evolution of the Bangong Meso-Tethys. *Int. Geol. Rev.* **56** (4), 430–447. https://doi.org/10.1080/00206814.2013.873356 (2014).
- 64. Wang, B. D. et al. Evolution of the Bangong-Nujiang Tethyan Ocean: insights from the geochronology and geochemistry of mafic rocks within ophiolites. *Lithos* 24 (15), 18–33. https://doi.org/10.1016/j.lithos.2015.07.016 (2016).
- 65. Tan, X. D. et al. New paleomagnetic results from the Lhasa block: revised Estimation of latitudinal shortening across Tibet and implications for dating the India-Asia collision. *Earth Planet. Sci. Lett.* **293** (3–4), 396–404. https://doi.org/10.1016/j.epsl.2010.03. 013 (2010).
- 66. Tong, Y. B. et al. Paleomagnetism of the upper cretaceous red-beds from the Eastern edge of the Lhasa Terrane: new constraints on the onset of the India-Eurasia collision and latitudinal crustal shortening in Southern Eurasia. *Gondwana Res.* 48, 86–100. https://doi.org/10.1016/j.gr.2017.04.018 (2017).
- 67. Sun, Z. M. et al. Paleomagnetism of late cretaceous sediments from Southern Tibet: evidence for the consistent palaeolatitudes of the Southern margin of Eurasia prior to the collision with India. *Gondwana Res.* 21 (1), 53–63. https://doi.org/10.1016/j.gr.2011.0 8.003 (2012).
- 68. Tong, Y. B. et al. The cenozoic rotational extrusion of the Chuan Dian fragments: new paleomagnetic results from paleogene red-beds on the southeastern edge of the Tibetan plateau. *Tectonophysics* 658, 46–60. https://doi.org/10.1016/j.tecto.2015.07.007 (2015).
- 69. Chen, W. W. et al. Combined paleomagnetic and geochronological study on cretaceous strata of the Qiangtang Terrane, central Tibet. *Gondwana Res.* 41, 93–109. https://doi.org/10.1016/j.gr2015.07.004 (2017).
- 70. Meng, J. et al. Paleomagnetism and detrital Zircon U-Pb geochronology of cretaceous redbeds from central Tibet and tectonic implications. *Geol. J.* 53 (5), 2315–2333. https://doi.org/10.1002/gi.3070 (2018).
- 71. Liu, W. et al. Geochemical characteristics and geological significance of Shamuluo formation argillaceous rocks in the Western part of the BangongCo-Nujiang suture zone. Acta Petrologica Et Mineral. 38 (1), 47–62 (2019).
- 72. Dewey, J. F. Orogeny can be very short. Earth, atmospheric. *Planet. Sci.* **102** (43), 15286–15293. https://doi.org/10.1073/pnas.0505 516102 (2005).
- 73. Dickinson, W. R. & Gehrels, G. E. Use of U-Pb ages of detrital zircons to infer maximum depositional ages of strata: A test against a Colorado plateau mesozoic database. Earth Planet. Sci. Lett. 288 (1–2), 115–125. https://doi.org/10.1016/j.epsl.2009.09.013 (2009).
- 74. Lei, C. Y. et al. Origin of Qushenla formation volcanic rocks in the Nawucuo area, Northern Tibet, and constraints on the subduction Polarity of the Bangong-Nujiang Tethys ocean. *J. Earth Sci.* 34, 467–486. https://doi.org/10.1007/s12583-020-1076-5 (2023).

- 75. Fan, J. J. et al. The evolution of the Bangong-Nujiang Neo-Tethys Ocean: evidence from Zircon U-Pb and Lu-Hf isotopic analyses of early cretaceous oceanic Islands and ophiolites. *Tectonophysics* 655 (1), 27–40. https://doi.org/10.1016/j.tecto.2015.04.019 (2015).
- Cawood, P. A., Hawkesworth, C. J. & Dhuime, B. Detrital Zircon record and tectonic setting. Geology 40 (10), 875–878. https://doi.org/10.1130/G32945.1 (2012).
- 77. Xu, Q. et al. Late Cretaceous-early paleogene rise of the Gandese magmatic Arc (south Tibet) from sea level to high mountains. GSA Bull. 135 (7–8), 1939–1954. https://doi.org/10.1130/B36438.1 (2022).
- 78. Wei, Y. Q. et al. Geochemistry, detrital Zircon geochronology and hf isotope of the clastic rocks in Southern Tibet: implications for the Jurassic-Cretaceous tectonic evolution of the Lhasa terrane. *Gondwana Res.* 78, 41–57. https://doi.org/10.1016/j.gr.2019.08.014 (2020).
- 79. Sun, Z. M. et al. Paleomagnetism of late cretaceous sediments from Southern Tibet: evidence for the consistent paleolatitudes of the Southern margin of Eurasia prior to the collision with India. *Gondwana Res.* 21 (1), 53–63. https://doi.org/10.1016/j.gr.2011.08.003 (2012).
- 80. Xing, L. Y. et al. Geochemistry and petrogenesis of sandstones and their basaltic interlayers of shexing formation from Linzhou basin, South Tibet. *Acta Petrologica Sinica*. **36** (9), 2729–2750. https://doi.org/10.18654/1000-0569/2020.09.08 (2020).
- 81. Wang, J. G. et al. From extension to tectonic inversion: Mid-Cretaceous onset of Andean-type orogeny in the Lhasa block and early topographic growth of Tibet. GSA Bull. 132 (11–12), 2432–2454. https://doi.org/10.1130/B35314.1 (2020).

Acknowledgements

This work was co-supported by the Second Tibetan Plateau Scientific Expedition (STEP) program (2019QZKK0704), the National Natural Science Foundation of China (Grants 42274097, 91855211, 42304092, 42074075, and 41774073). And the authors thank Wu, J. Y., Wang, J. W., Wang, B. F., and Xu, P. X. for their assistance in the field work. And thanks to the reviewers for their corrections.

Author contributions

(A) wrote the main manuscript text. (B) and (C) revised the manuscript. (D) provided the writing idea. E., F. and G. provided the rock samples and some data information. H. carried out the experiments. All authors reviewed the manuscript.

Declarations

Competing interests

The authors declare no competing interests.

Additional information

Correspondence and requests for materials should be addressed to Q.C. or H.W.

Reprints and permissions information is available at www.nature.com/reprints.

Publisher's note Springer Nature remains neutral with regard to jurisdictional claims in published maps and institutional affiliations.

Open Access This article is licensed under a Creative Commons Attribution-NonCommercial-NoDerivatives 4.0 International License, which permits any non-commercial use, sharing, distribution and reproduction in any medium or format, as long as you give appropriate credit to the original author(s) and the source, provide a link to the Creative Commons licence, and indicate if you modified the licensed material. You do not have permission under this licence to share adapted material derived from this article or parts of it. The images or other third party material in this article are included in the article's Creative Commons licence, unless indicated otherwise in a credit line to the material. If material is not included in the article's Creative Commons licence and your intended use is not permitted by statutory regulation or exceeds the permitted use, you will need to obtain permission directly from the copyright holder. To view a copy of this licence, visit http://creativecommons.org/licenses/by-nc-nd/4.0/.

© The Author(s) 2025